Cell Reports

Article

Staphylococcus aureus skin colonization is mediated by SasG lectin variation

Graphical abstract

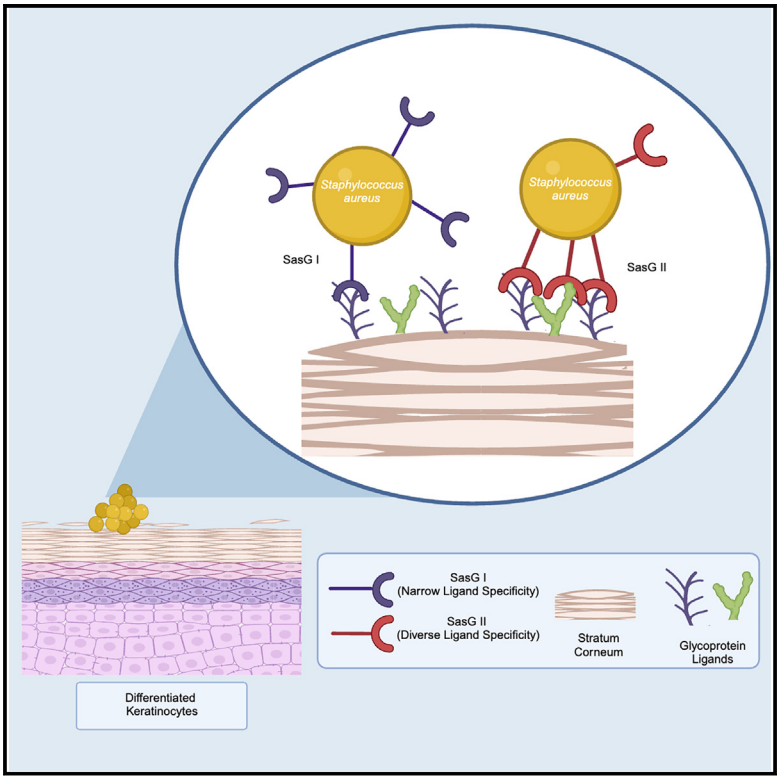

Highlights

- There are two major divergent SasG alleles in *S. aureus*, SasG-I and SasG-II
- SasG-II contains a nonaromatic arginine residue in the lectin-binding pocket
- SasG-II has a different adhesion profile than SasG-I and binds a broader variety of ligands

Authors

Krista B. Mills, Joseph J. Maciag, Can Wang, ..., Paul D. Fey, Andrew B. Herr, Alexander R. Horswill

Correspondence

alexander.horswill@cuanschutz.edu

In brief

Mills et al. show that *Staphylococcus aureus* surface protein G (SasG) has two major divergent alleles, SasG-I and SasG-II. SasG-II has a broader binding profile than SasG-I, which confers an advantage to these *S. aureus* SasG-II-expressing strains in colonizing human skin.

Mills et al., 2024, Cell Reports *43*, 114022
April 23, 2024
https://doi.org/10.1016/j.celrep.2024.114022

CellPress

Cell Reports

CellPress
OPEN ACCESS

Article

Staphylococcus aureus skin colonization is mediated by SasG lectin variation

Krista B. Mills,[1] Joseph J. Maciag,[2,10] Can Wang,[3,10] John A. Crawford,[4] Timothy J. Enroth,[1] Klara C. Keim,[1] Yves F. Dufrêne,[3] D. Ashley Robinson,[4,5] Paul D. Fey,[6] Andrew B. Herr,[2,7,8] and Alexander R. Horswill[1,9,11,*]

[1]Department of Immunology and Microbiology, University of Colorado Anschutz Medical Campus, Aurora, CO, USA
[2]Division of Immunobiology, Cincinnati Children's Hospital Medical Center, Cincinnati, OH, USA
[3]Louvain Institute of Biomolecular Science and Technology, UCLouvain, Louvain-la-Neuve, Belgium
[4]Department of Cell and Molecular Biology, University of Mississippi Medical Center, Jackson, MS, USA
[5]Center for Immunology and Microbial Research, University of Mississippi Medical Center, Jackson, MS, USA
[6]Department of Pathology and Microbiology, University of Nebraska Medical Center, Omaha, NE, USA
[7]Division of Infectious Diseases, Cincinnati Children's Hospital Medical Center, Cincinnati, OH, USA
[8]Department of Pediatrics, University of Cincinnati College of Medicine, Cincinnati, OH, USA
[9]Department of Veterans Affairs, VA Eastern Colorado Healthcare System, Aurora, CO, USA
[10]These authors contributed equally
[11]Lead contact
*Correspondence: alexander.horswill@cuanschutz.edu
https://doi.org/10.1016/j.celrep.2024.114022

SUMMARY

Staphylococcus aureus causes the majority of skin and soft tissue infections, but this pathogen only transiently colonizes healthy skin. However, this transient skin exposure enables *S. aureus* to transition to infection. The initial adhesion of *S. aureus* to skin corneocytes is mediated by surface protein G (SasG). Here, phylogenetic analyses reveal the presence of two major divergent SasG alleles in *S. aureus*: SasG-I and SasG-II. Structural analyses of SasG-II identify a nonaromatic arginine in the binding pocket of the lectin subdomain that mediates adhesion to corneocytes. Atomic force microscopy and corneocyte adhesion assays indicate that SasG-II can bind to a broader variety of ligands than SasG-I. Glycosidase treatment results in different binding profiles between SasG-I and SasG-II on skin cells. In addition, SasG-mediated adhesion is recapitulated using differentiated N/TERT keratinocytes. Our findings indicate that SasG-II has evolved to adhere to multiple ligands, conferring a distinct advantage to *S. aureus* during skin colonization.

INTRODUCTION

The opportunistic pathogen *Staphylococcus aureus* is a common asymptomatic colonizer in humans, but it is also the predominant cause of skin and soft tissue infections.[1] Approximately 20% of the human population are persistently colonized by *S. aureus,* most commonly in the anterior nares, whereas 30% are transiently colonized.[2,3] *S. aureus* infections usually occur in individuals who are already colonized.[3,4] Despite causing ~76% of skin and soft tissue infections,[5] *S. aureus* only colonizes ≤5% of the skin of otherwise healthy adults.[6] A trifecta of intact barrier, immune system, and commensal microbiota maintains skin homeostasis and keeps *S. aureus* colonization rates low. However, dysbiosis or breaks in the skin barrier can lead to increased colonization levels and subsequent infection.[7–9] When skin homeostasis is compromised, *S. aureus* can deploy virulence factors that enable immune evasion and tissue invasion, further exacerbating inflammation and disease.[10–12] Identifying the mechanisms by which *S. aureus* colonizes healthy skin could open avenues for therapeutic development to prevent and treat infection in colonized individuals.

S. aureus skin colonization begins with initial adhesion, which is mediated by various cell wall-anchored (CWA) proteins.[11,13–15] In particular, surface protein G (SasG) is known to be important in *S. aureus* adhesion to healthy human corneocytes on the skin,[15–17] as well as adhesion to nasal epithelial cells and in biofilm formation.[18,19] SasG is a large sortase-anchored protein that is part of the G5-E-repeat family of adhesins.[11] The structure of this protein consists of an N-terminal A domain encompassing an intrinsically disordered region and L-type lectin, a B domain with highly conserved, serial B-repeats containing G5-repeat and E-spacer subdomains[11,16,18] and a proline/glycine-rich stalk region extending to the C terminus.[20] SasG is orthologous to accumulation-associated protein (Aap) in *S. epidermidis*, and SasG homologs are expressed in other species of staphylococci as well.[15] Similar to SasG, Aap has been found to be important in *S. epidermidis* adhesion to healthy human corneocytes.[15,16]

Previous studies have elucidated the role of the A domain, specifically the L-type lectin subdomain, in Aap and SasG-mediated adhesion to corneocytes on healthy human skin.[15–17] L-type lectins exhibit glycan-binding specificity that can vary significantly depending on the lectin.[21] Although the specific ligand for Aap and SasG is still unknown, recent data

have indicated that the ligand is most likely a glycoprotein. Roy et al.[15] demonstrated that healthy human skin corneocytes treated with the glycosidases peptide:*N*-glycosidase (PNGase) and *O*-glycosidase significantly reduced *S. epidermidis* adhesion, suggesting that these glycan linkages are important for adhesion to the host ligand. A glycan array performed by Maciag et al.[16] supported these data and found that the highest-affinity hits for the Aap lectin included N-linked glycans containing Gal-GlcNAc alternating repeats (poly-*N*-acetyllactosamine). Furthermore, Maciag et al. identified key aromatic residues within the glycan-binding pockets of the Aap and SasG lectins, which likely bind glycans through stacking interactions. These key aromatic residues are approximately in the same structural position, Y580 for Aap and W392 for SasG, and mutation of these residues to alanine abrogated the binding of these lectins to *N*-acetyl-D-lactosamine and 3′-sialyl-*N*-acetyllactosamine as determined via isothermal titration calorimetry (ITC).[16] Similarly, preincubating corneocytes from healthy human skin with purified lectins from Aap and SasG significantly reduced adhesion of both *S. epidermidis* and *S. aureus*, whereas the mutated lectins did not affect adhesion,[16] demonstrating that Aap and SasG bind to the ligand via these key residues in the lectin subdomain.

The ability of purified lectins from both Aap and SasG to bind lactosamine derivatives and reduce adhesion of both *S. epidermidis* and *S. aureus* to corneocytes suggests that these species may compete for adhesion to the same ligand on healthy human skin. However, in an *S. epidermidis*-dominated skin environment[22,23] that is hostile to *S. aureus*, much has yet to be elucidated as to what makes SasG unique and able to establish a colonization niche. Here, we use phylogenetic analyses to demonstrate the presence of two divergent allelic types of SasG, with each type represented by full-length and truncated forms, within *S. aureus*. We demonstrate that SasG-II may bind to multiple ligands, based on evidence that includes the SasG-II lectin structure and a lectin alignment comparison to SasG-I, adhesion studies on corneocytes from healthy human skin and immortalized N/TERT keratinocytes, and nanoimaging of corneocytes using SasG-I and SasG-II *S. aureus* single-cell probes.

RESULTS

The SasG A domain is variable in *S. aureus*

Variability in the repertoire of sortase-attached adhesins is common on the surface of *S. aureus*.[24] SasG in particular has been noted as having significant strain-level diversity in gene (*sasG*) presence, expression level, and function.[18,25] We realized that *S. aureus* strains expressing full-length SasG, such as well-known strains COL and 502a in clonal complex 8 (CC8) and CC5, and MW2 in CC1, have considerable divergence in the A domain sequence. Considering that the SasG A domain has been recently linked to corneocyte adhesion,[15,17] we reasoned that the sequence differences could affect *S. aureus* skin colonization.

Full-length SasG from methicillin-resistant *S. aureus* (MRSA) strain COL has a lectin domain that is structurally similar to that of *S. epidermidis* Aap, as we recently reported.[16] We have called this form of SasG type I or SasG-I. In contrast, the A domain lectin in MRSA strain MW2 is only 67.2% identical at the protein level. We called this form of SasG type II or SasG-II. The rest of the protein content in both full-length SasG forms is fairly similar to the B-repeat region containing G5 and E spacers and a C-terminal wall/membrane spanning region with an LPKTG sortase motif (Figure S1A). In this initial analysis, we also determined that some strains encoding SasG-I had an intact A domain and a frameshift mutation at the start of the B domain. This includes strains such as N315[26] and LAC[19] that belong to USA100-related and USA300 lineages, respectively. We called this mutated form of SasG-I "truncated SasG-I." Some strains with SasG-II also encode a truncated protein; however, this form occurs less frequently among *S. aureus* strains and was not investigated further.

Both the Aap and SasG-I lectins have a key active site aromatic residue that has been linked to glycan binding and corneocyte adhesion, which is Y580 in Aap and W392 in SasG-I.[16] Based on an alignment of the SasG-I and SasG-II lectins, this aromatic residue is missing in SasG-II and is replaced with nonaromatics (Figure S1B). Other secondary structure elements are similar, as expected given that both adopt β sandwich L-type lectin folds. Based on our previous analysis of the SasG-I and Aap lectin structures,[16] most of the key residues in the vicinity of the glycan-binding site (shortly after β17) are conserved between SasG-I and SasG-II, with one important exception, as described below.

Phylogenetic analyses reveal the depth of SasG variation

Building on our preliminary observations, we further investigated SasG variation using a phylogenetically diverse set of *S. aureus* isolates for which whole-genome sequences were available.[27] These 574 isolates belonged to 39 clonal complexes (Figure 1A). Among these isolates, SasG was represented by 3 approximately evenly distributed groups: 191 full-length SasG, 194 truncated SasG, and 189 missing SasG. Phylogenetic analysis of the aligned full-length SasG sequences confirmed that the species has two divergent allelic types with 99 inferred amino acid substitutions between them (Figure 1C, long branch separating the two types). Among the full-length SasG sequences, there were 91 unique SasG sequences with 11 distinct amino acid lengths of sequence that could be attributed to the B-repeat region. The individual B-repeats were exactly 128 amino acids in length, and 11 differently sized repeat arrays were detected among the full-length SasG sequences. The distribution of B-repeats among the two full-length SasG types was significantly different ($\chi^2 = 57.3$, df = 10, $p < 0.0001$), with a more even number of B-repeats among the type II isolates compared to the type I isolates (Figure 1B).

Different isolates of a given clonal complex always had the same SasG type. However, at least four changes of SasG types are inferred based on parsimony analysis of the type distribution on the *S. aureus* phylogeny. The two SasG types correlate perfectly with amino acid polymorphisms in the L-type lectin-binding region: W392 for SasG-I and R394 for SasG-II. Since polymorphisms in these alignment positions correlated perfectly with the full-length SasG types, these two amino acids were used to type the truncated SasG sequences. This typing allowed

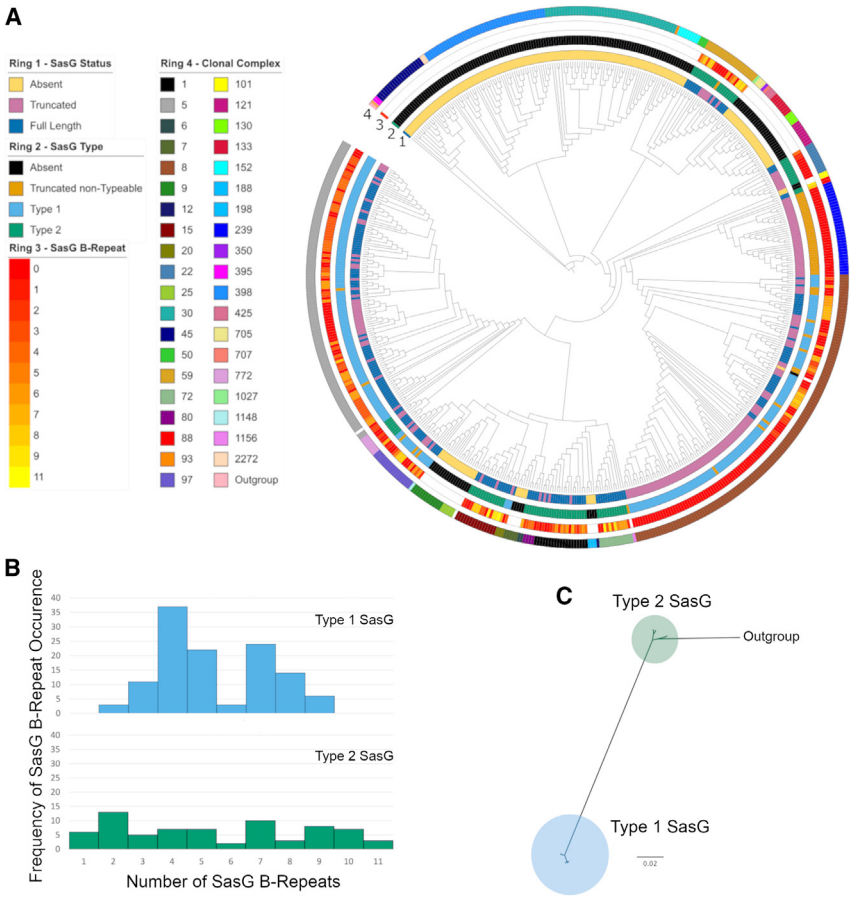

Figure 1. SasG variation in the context of *S. aureus* phylogenetic diversity

(A) Maximum likelihood phylogenetic tree of 574 *S. aureus* isolates based on their proteome. For each isolate, SasG status is mapped to ring 1, SasG type (defined in B) is mapped to ring 2, SasG B-repeat number is mapped to ring 3, and the clonal complex of the isolate is mapped to ring 4.

(B) Histograms of SasG B-repeats from both SasG allelic types.

(C) Maximum likelihood phylogenetic tree of SasG from 191 aligned full-length sequences identifies 2 SasG allelic types.

for an additional parsimony analysis that identified a minimum of 27 changes between a predicted functional SasG (full-length or typed-truncated sequence) and a predicted nonfunctional SasG (missing or untyped-truncated sequence). The clonal complexes CC5 and CC8, which are clinically important,[28–30] both encode SasG-I, but CC5 has mostly full-length forms and CC8 has mostly truncated forms. SasG-II is encoded by CC1 (e.g., MRSA strain MW2), as well as CC15, CC22, CC59, CC72, and others. SasG-II in these CCs are mostly full-length, although some strains do rarely harbor truncated SasG-II.

The SasG-II lectin contains a nonaromatic residue in the glycan-binding pocket

The crystal structure of SasG-II lectin was solved at 1.88 Å (Table S1), revealing an overall architecture that is nearly identical to the L-type lectin folds of SasG-I, Aap, and Pls[16,31] (Figure 2A). Similar to these related lectin domains, SasG-II has an atypical *trans* conformation of the central D241 residue, a structural Ca^{2+} ion, and three relatively long loops at the top of the domain. However, both Aap and SasG-I lectins feature a sharp bend in the main chain after strand β17 that positions an aromatic residue at the base of the glycan-binding pocket (i.e., Aap Y580 and SasG-I W392) (Figure 2B). In contrast, SasG-II fails to adopt the sharp bend at the end of β17, which therefore positions the side chain of R394 in approximately the same position as the SasG-II main chain after the bend. The arginine at this position is actually conserved between SasG-I and SasG-II, but the sharp bend in the main chain of SasG-I causes the equivalent R391 to extend toward the top of the lectin domain, far from the binding pocket, and positions W392 within the binding pocket instead (Figure 2C). Likewise, the Q395 residue in SasG-II (corresponding to W392 in SasG-I) points in the opposite direction to R394 in a region of the protein that is highly solvent exposed (Figure 2C). It seems likely that SasG-I and Aap adopt the sharp bend in the main chain after β17 to reduce exposure of the equivalent aromatic residues (W392 or Y580) to solvent, which would be entropically unfavorable. Instead, the main chain bend orients those aromatic residues toward the binding site pocket region, which is more protected from solvent. As a result of these structural differences, SasG-II forms a surface pocket similar to the glycan-binding sites of the other lectins, but it does not contain an aromatic residue that could form a stacking interaction with a glycan ligand (Figure 2D).

Multiparametric nanoimaging using single bacterial probes indicates SasG-II binds a broader variety of ligands than SasG-I

To compare SasG-I- and SasG-II-mediated adhesion at the single-molecule level and further explore the possibility of SasG-II binding multiple ligands, we determined the strength of adhesion between a single living bacterial cell and human corneocytes using multiparametric atomic force microscopy (AFM) imaging.[32] Bacterial cells not expressing SasG (*S. carnosus*-pALC2073 empty vector [EV]) did not show any adhesion (Figure 3), similar to a colloidal probe (Figures 3 and S2). Bacterial cells expressing SasG-II (*S. carnosus-sasG*$_{MW2}$) showed strong adhesion forces ranging from 500 to 5,000 pN, with a most frequently observed force of ~1,000 pN, that were densely and widely distributed across the corneocyte surface (Figures 3 and S3). It is likely that the 1,000-pN force corresponds to a single interaction, whereas larger forces represent multiple bonds, possibly of a different molecular nature. Force curves (Figure 3B, insets)

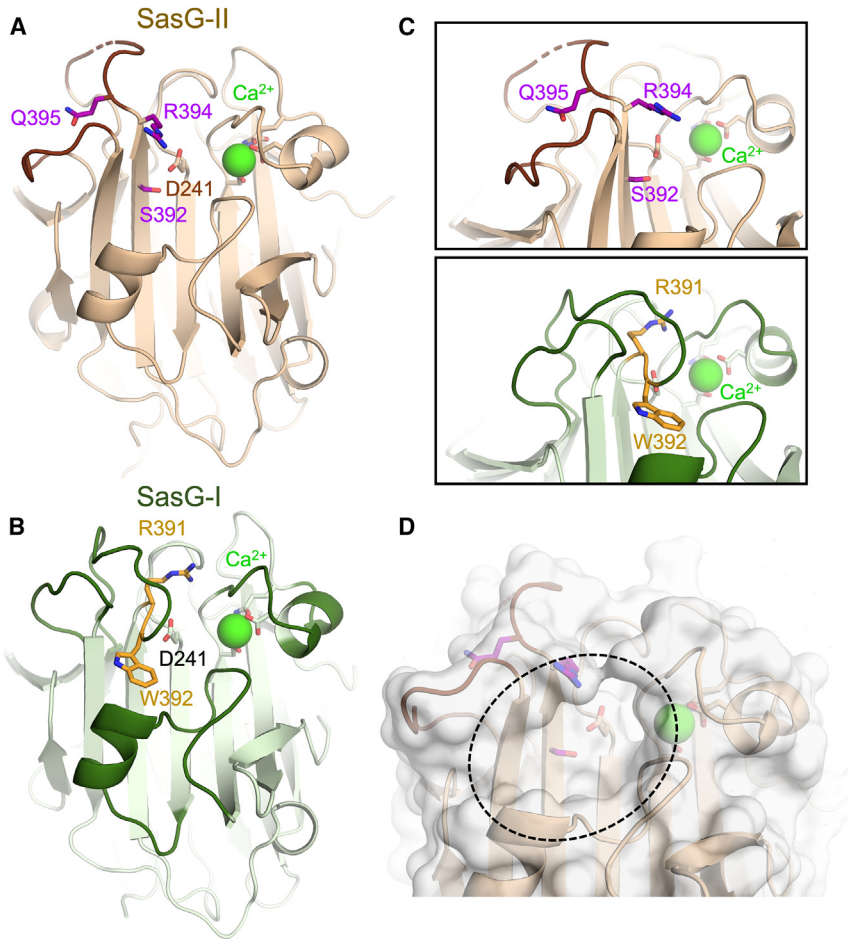

Figure 2. The SasG-II lectin contains a unique nonaromatic residue in the glycan-binding pocket

(A) Crystal structure of the SasG-II lectin showing the structural Ca^{2+} ion, the conserved central D241 residue that adopts an atypical *trans* conformation, and the side chains of S392, R394, and Q395 near the end of β17.

(B) Comparative view of SasG-I in the same orientation. Residues R391 and W392 are analogous to R394 and Q395 in SasG-II; note the distinct positioning of corresponding residues W392 (SasG-I) and Q395 (SasG-II).

(C) Close-up view of the region near the end of β17, rotated by ∼45° from (A) and (B). Note the sharp bend of the main chain near R391 in SasG-I that is not observed in SasG-II.

(D) Surface view of SasG-II showing the putative binding pocket lacking an aromatic residue at its base.

exhibited sawtooth patterns with multiple equally spaced peaks, originating from the unfolding of individual E and G5 repeats of the B region. This was followed by a single strong peak resulting from the rupture of the A domain-corneocyte interaction. Rupture forces of ∼2,000 pN (Figure 3B) may result from two SasG-II adhesins binding to two receptors on the surface of the corneocyte. This multivalency is likely to enhance bacterial adhesion. The detection frequency of 27% demonstrates that the SasG-II ligand(s) are present at high density. SasG-I-expressing cells also showed many adhesion forces at ∼1,000 pN, yet with a much lower detection frequency of ∼7% (Figures 3 and S4). This indicates that both adhesins strongly bind their skin ligands, yet SasG-II seems to bind a broader variety of ligands.

Purified glycans do not affect SasG-II-mediated adhesion to corneocytes

As we have shown previously, the Aap and SasG-I lectins were both able to bind purified *N*-acetyl-D-lactosamine via ITC.[16] Using ITC, we investigated whether SasG-II would also bind *N*-acetyl-D-lactosamine, and found that the SasG-II lectin did not bind (Figure S5A). This was functionally validated in a corneocyte adhesion assay, where preincubation with a serial 2-fold dilution of *N*-acetyl-D-lactosamine ranging from 1,000 to 62.5 μM did not affect SasG-II-expressing *S. carnosus-sasG*$_{MW2}$ adhesion to corneocytes (Figures S5B and S5C). Similarly, preincubation with a serial 2-fold dilution of 3′-sialyl-*N*-acetyllactosamine ranging from 100 to 6.25 μM (10-fold lower dilutions than was used with *N*-acetyl-D-lactosamine) did not affect SasG-II-expressing *S. carnosus-sasG*$_{MW2}$ adhesion to corneocytes (Figures S5D and S5E). In contrast, adhesion of SasG-I-expressing *S. carnosus*/pALC2073-*sasG*$_{COL}$ was strongly inhibited by 125 μM *N*-acetyl-D-lactosamine or by 12.5 μM 3′-sialyl-*N*-acetyllactosamine.[16] These data collectively suggest that SasG-II is unique from Aap and SasG-I in that it may bind distinct glycan ligands on the corneocyte receptor or perhaps that it binds the protein portion of the receptor without engaging the glycan moieties.

SasG-I- and -II-mediated adhesion to corneocytes shows differential responses upon treatment with glycosidases

To narrow down possible ligand targets for SasG-I and SasG-II and further investigate binding differences between the two types, corneocytes were preincubated with glycosidases. Protein glycosylation has been postulated to be important for epidermal differentiation, as well as desquamation, hydration, and adhesion/cohesion of the stratum corneum.[33,34] The most common types of glycans found on healthy human skin are variations of complex N-linked glycans and mucin-like core 1 and core 2 O-linked glycans.[34–37] Seven different glycosidases were tested, including endoglycosidases and exoglycosidases: PNGase F (cleaves between the innermost GlcNAc and asparagine residues of high-mannose, hybrid, and complex oligosaccharides), *O*-glycosidase (catalyzes removal of core 1 and 3 O-linked disaccharides from glycoproteins), α1-2,3,6 mannosidase (catalyzes the hydrolysis of terminal, nonreducing α1-2, α1-3, and α1-6 linked mannose residues from

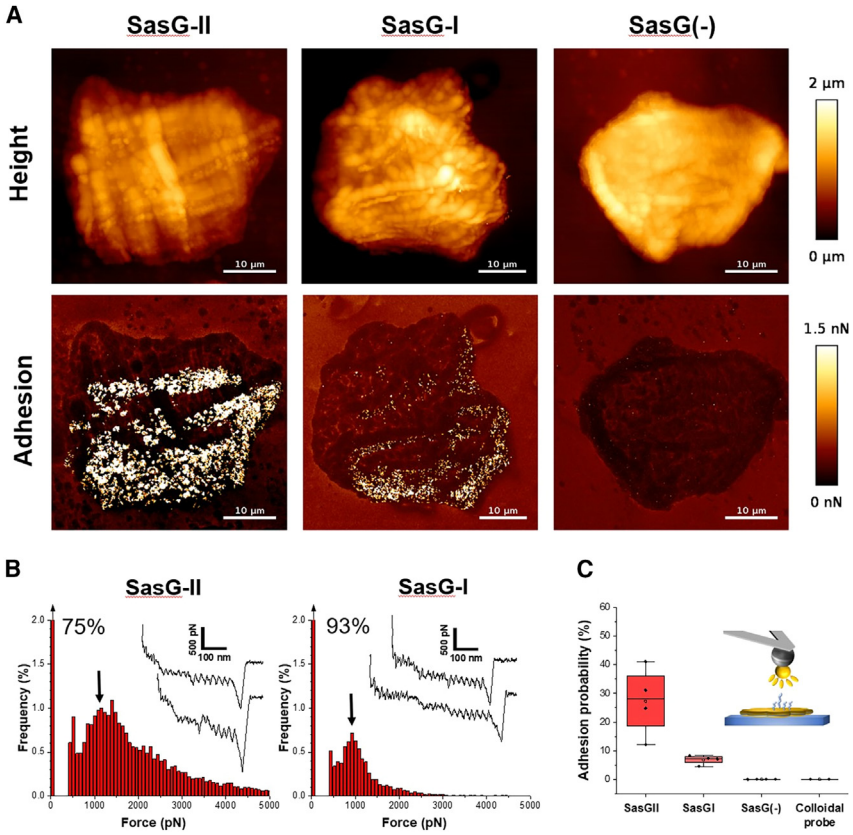

Figure 3. Multiparametric nanoimaging using single bacterial probes indicates SasG-II binds a broader variety of ligands than SasG-I

(A) Height images (top) and adhesion images (bottom) of corneocytes recorded in PBS using a SasG-II, SasG-I, or EV (SasG[-]) cell probe (see also Figures S2–S4). These images are representative of at least 3 independent experiments.

(B) Histograms of adhesion forces registered on whole corneocytes (total of n = 9,590 curves for 1 representative SasG-II probe; n = 2,532 curves for 1 representative SasG-I probe). Representative force curves are shown as insets. The arrows at the top left of the histograms stand for the nonadhesive events.

(C) Boxplot comparing adhesion probabilities for SasG-II (n = 4 from 3 independent bacterial cultures), SasG-I (n = 4 from 2 independent bacterial cultures), SasG(−) (n = 4 from 2 independent bacterial cultures) or colloidal (n = 2) probes. For more data, see Figures S2–S4.

oligosaccharides), α1-3,4 fucosidase (catalyzes the hydrolysis of terminal, nonreducing α1-3 and α1-4 linked fucose residues from oligosaccharides and glycoproteins), β-*N*-acetylglucosaminidase S (catalyzes the hydrolysis of terminal, nonreducing β-*N*-acetylglucosamine residues from oligosaccharides), β1-4 galactosidase S (catalyzes the hydrolysis of terminal, nonreducing β1-4 linked galactose residues from oligosaccharides), and α2-3,6,8 neuraminidase (catalyzes the hydrolysis of α2-3, α2-6, and α2-8 linked sialic acid residues from glycoproteins and oligosaccharides).

We predicted that SasG-I-mediated adhesion would be similar to our previous results with Aap[15] and would be reduced upon glycosidase treatment with the endoglycosidases PNGase F and *O*-glycosidase, as well as α2-3,6,8 neuraminidase, and the exoglycosidases α1-3,4 fucosidase and β1-4 galactosidase S. Indeed, preincubation with all five of these glycosidases resulted in significantly reduced adhesion of *S. carnosus-sasG*$_{COL}$ compared to buffer controls, whereas the exoglycosidases α1-2,3,6 mannosidase and β-*N*-acetylglucosaminidase S did not affect adhesion (Figures 4A–4G). This suggests that linkages between the innermost N-acetylgalactosamine (GlcNAc) and asparagine residues of oligosaccharides, as well as core 1 and 3 O-linkages are important in SasG-I mediated adhesion, and that 5-*N*-acetylneuraminic acid, fucose, and galactose may be important in the SasG-I ligand structure.

Considering the inability of the SasG-II lectin to bind lactosamine (Figure S5A), we predicted that SasG-II may bind different terminal sugar residues on corneocytes than SasG-I. Using the same corneocyte adhesion assay, only preincubation with β-*N*-acetylglucosaminidase S and β1-4 galactosidase S resulted in a reduction of *S. carnosus-sasG*$_{MW2}$ adhesion (Figures 4A–4G). This indicates that terminal β-*N*-acetylglucosamine and galactose may be important in the SasG-II ligand structure. The only glycosidase that resulted in both reduced SasG-I and SasG-II adhesion was β1-4 galactosidase S, suggesting that galactose may be important in the structure of a shared ligand between SasG-I and SasG-II. These results further suggest that SasG-II binds a different type of glycan ligand than SasG-I on the corneocyte receptor.

SasG-II-mediated adhesion is mediated by the lectin subdomain and may bind the same ligand as Aap and SasG-I

To investigate the possibility of a shared ligand between SasG-I and SasG-II, we sought to determine if purified lectins from Aap, SasG-I, and SasG-II could cross-inhibit SasG-II-mediated adhesion to corneocytes. Preincubating/blocking corneocytes from healthy human skin with 5-μM purified lectin domains from Aap, SasG-I, and SasG-II significantly reduced SasG-II-expressing MRSA MW2 adhesion, whereas purified lectins with the key residues mutated—Aap ΔY580A and SasG-I ΔW392A—did not affect adhesion (Figures 5A and 5B). We then investigated whether this would hold true in the model surrogate organism *S. carnosus*, which does not natively adhere to corneocytes.[17] Expressing SasG in *S. carnosus* acts as an ideal model for testing protein-specific adhesion since there are no other adhesins that could affect corneocyte binding. Similar to *S. aureus*, adhesion of *S. carnosus* expressing SasG-II on plasmid pALC2073 was significantly reduced when preincubated/blocked with purified lectins from Aap and SasG-I, but was not affected by preincubation with Aap ΔY580A or

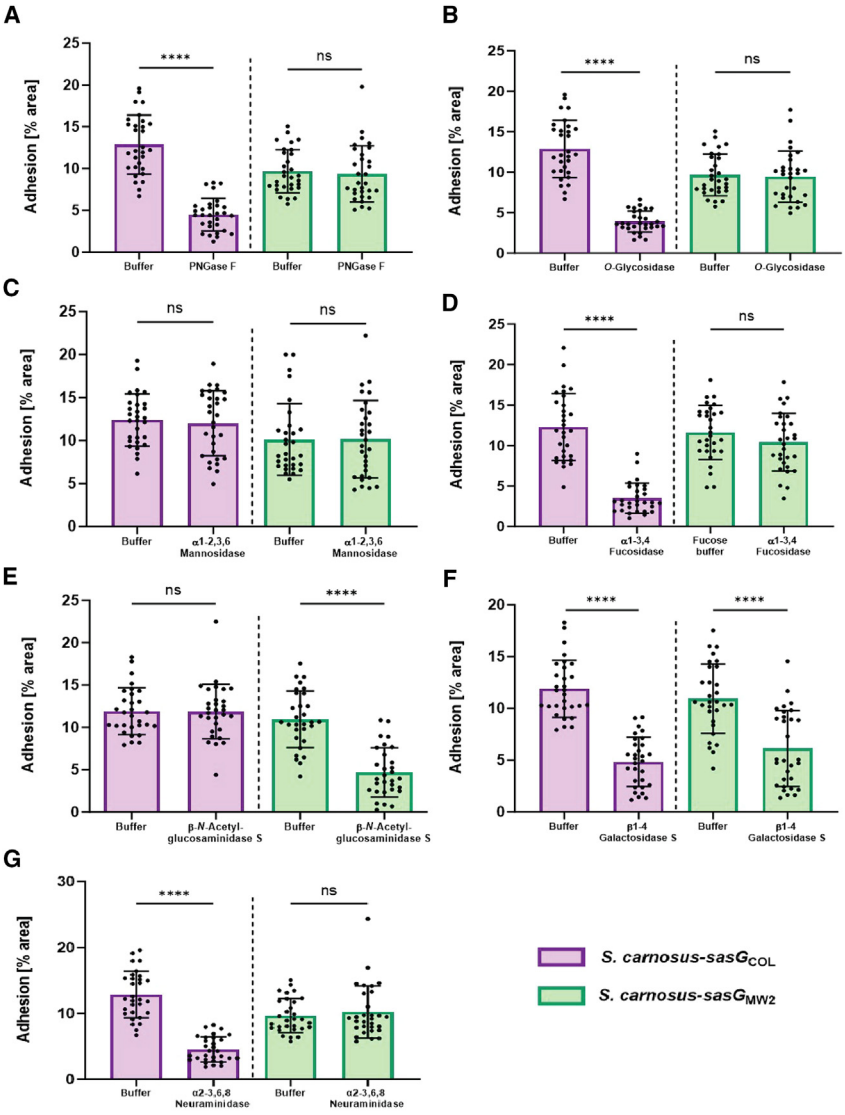

Figure 4. SasG-I- and -II-mediated adhesion to corneocytes shows differential responses upon treatment with glycosidases

S. carnosus-sasG$_{COL}$ (SasG-I) and *S. carnosus-sasG*$_{MW2}$ (SasG-II) were tested for adhesion to corneocytes following preincubation with (A) PNGase F, (B) *O*-glycosidase, (C) α1-2,3,6 mannosidase, (D) α1-3,4 fucosidase, (E) β-*N*-acetylglucosaminidase S, (F) β1-4 galactosidase S, and (G) α2-3,6,8 neuraminidase. The percent area of adhesion in 10 images from 3 independent experiments (n = 30) was measured with Fiji ImageJ and analyzed in GraphPad Prism. Statistical significance was analyzed using the unpaired t test or nonparametric Mann-Whitney test for data with nonnormal distribution (ns, not significant; ****$p < 0.0001$).

SasG-I ΔW392A, validating the findings in *S. aureus* (Figures 5C and 5D). These data suggest that SasG-II may bind to the same host ligand as SasG-I and Aap. Alternatively, SasG-II could be binding elsewhere on the corneocyte receptor, sterically blocking SasG-I and Aap from binding.

We then investigated whether purified SasG-II could cross-inhibit SasG-I- and Aap-mediated adhesion to corneocytes. Purification of type II full-length and A domain SasG from MRSA MW2 was characterized previously.[19] Preincubation/blocking with 100 μg/mL purified A domain and full-length SasG-II significantly reduced the adhesion of *S. epidermidis* to corneocytes (Figures 5E and 5F). Likewise, preincubation/blocking with 100 μg/mL purified A domain and full-length SasG-II significantly reduced SasG-I-expressing *S. carnosus-sasG*$_{COL}$ adhesion to corneocytes (Figures 5G and 5H). These findings suggest that the SasG-II mode of binding to the corneocyte receptor enables competition with staphylococci expressing Aap or SasG-I.

SasG-I- and SasG-II-mediated adhesion to differentiated N/TERT keratinocytes following treatment with glycosidases suggests complex N-linked glycans and core 2 *O*-glycans may be important for SasG-I and SasG-II binding

To validate the adhesion data seen on corneocytes and explore whether SasG could be used for invasion, we used a live, immortalized, N/TERT-2G keratinocyte cell culture model. N/TERT keratinocytes can undergo terminal differentiation, allowing for the presence of multiple keratinocyte layers with a desquamated stratum corneum. Terminally differentiated N/TERT keratinocytes with a stratum corneum were incubated with *S. carnosus*-pALC2073 EV (negative control), SasG-I-expressing *S. carnosus-sasG*$_{COL}$, SasG-II-expressing *S. carnosus-sasG*$_{MW2}$, and SasG-II-expressing *S. carnosus* with the A domain deleted (*S. carnosus-sasG*$_{MW2\Delta A}$).[17] Similar to what was seen in the corneocyte adhesion assays, both SasG-I- and SasG-II-expressing *S. carnosus* strains adhered significantly more to differentiated N/TERTs than the EV and SasG-II A domain mutant controls (Figures 6A and 6B). To determine whether SasG could be used not only in initial adhesion to the stratum corneum but also for adherence to the more basal, actively dividing keratinocyte layers, these same strains were then tested for adhesion to an undifferentiated monolayer of N/TERT keratinocytes. Conversely, none of the strains adhered differently in a statistically significant manner (Figures 6C and 6D). The difference in adhesion for SasG-I-expressing *S. carnosus-sasG*$_{COL}$ and SasG-II-expressing *S. carnosus-sasG*$_{MW2}$ on differentiated vs. undifferentiated N/TERT keratinocytes is illustrated in Figure 6E, where much lower adhesion is seen for both strains in undifferentiated N/TERT keratinocytes than differentiated N/TERT keratinocytes containing a stratum corneum. These data indicate that SasG is used by *S. aureus* for initial adhesion to the outermost layer of

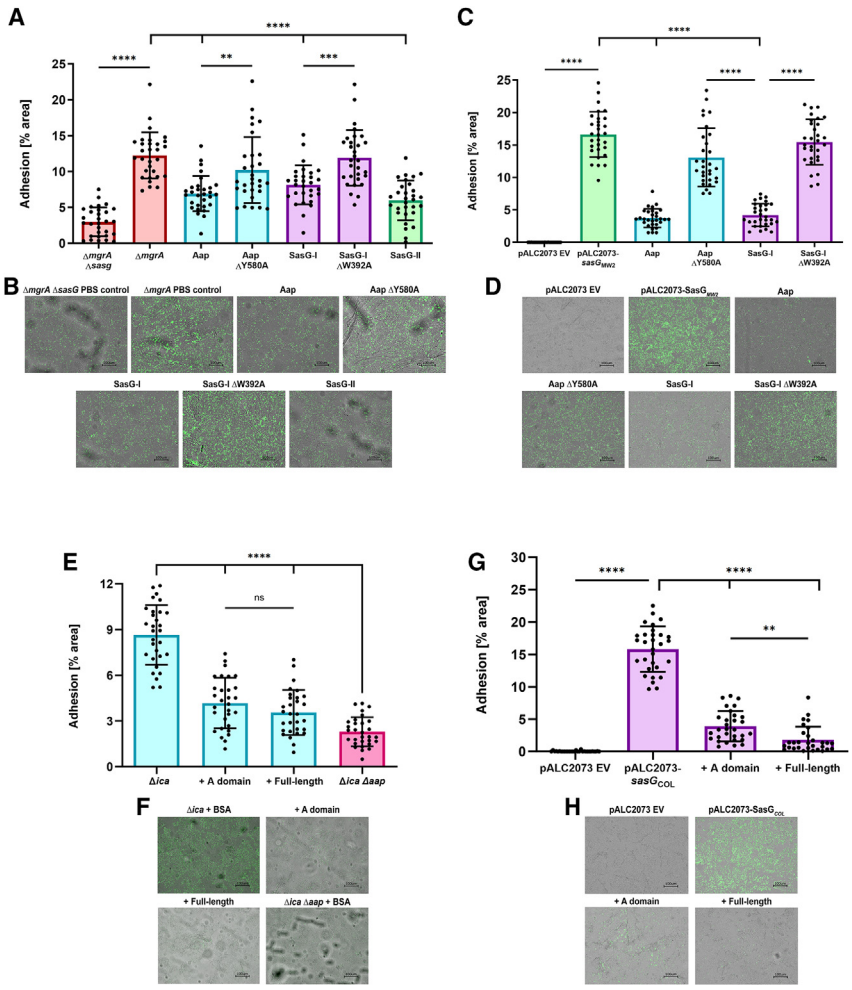

Figure 5. SasG-II-mediated adhesion is mediated by the lectin subdomain and may bind the same ligand as Aap and SasG-I

(A) SasG-II-expressing MRSA MW2 Δ*mgrA* (where *mgrA* repression allows for SasG expression[19]) was tested for adhesion to healthy human corneocytes after preincubation/blocking with 5 μM purified lectins. MRSA MW2 Δ*mgrA* Δ*sasG* was used as a negative control strain. **p = 0.0019.

(C) SasG-II-expressing *S. carnosus-sasG*$_{MW2}$ was tested for adhesion to healthy human corneocytes after preincubation/blocking with 5 μM purified lectins. *S. carnosus*-pALC2073 EV was used as a negative control strain.

(E) *S. epidermidis* Δ*ica* (where Δ*ica* acts as a wild-type strain because it does not interfere with bacterium-cell adherence[15]) was tested for adhesion to corneocytes following preincubation/blocking with 100 μg/mL purified full-length or A domain SasG-II. *S. epidermidis* Δ*ica* Δ*aap* was used as a negative control strain.

(G) SasG-I-expressing *S. carnosus-sasG*$_{COL}$ was tested for adhesion to healthy human corneocytes after preincubation/blocking with 100 μg/mL purified full-length or A domain SasG-II. *S. carnosus*-pALC2073 EV was used as a negative control strain. **p = 0.0091.

(B, D, F, and H) Representative bright-field (representing corneocytes) and green-channel (representing GFP-expressing bacteria) overlay microscopy images of experimental groups tested in (A), (C), (E), and (G), respectively.

(A–H) The percent area of adhesion in 10 images from 3 independent experiments (n = 30) was measured with Fiji ImageJ and analyzed in GraphPad Prism. Statistical significance was analyzed using ordinary 1-way ANOVA (***p = 0.0002; ****p < 0.0001). Scale bar: 100 μm.

the skin to establish a colonization niche, but not to infiltrate deeper layers of the epidermis.

With the understanding that the ligand(s) to SasG exist(s) on the stratum corneum, we then investigated whether the glycosidase treatment on corneocytes would reveal similar glycan ligand targets on live cells. *S. carnosus-sasG*$_{MW2}$ and *S. carnosus-sasG*$_{COL}$ were tested for adhesion to differentiated N/TERT keratinocytes following preincubation with glycosidases β-*N*-acetylglucosaminidase S and β1-4 galactosidase S. Similar to the corneocyte data, treatment with these two glycosidases reduced *S. carnosus-sasG*$_{MW2}$ adhesion to differentiated N/TERT keratinocytes. Although not statistically significant, β-*N*-acetylglucosaminidase S exhibited a reduced adhesion trend for *S. carnosus-sasG*$_{MW2}$, and this reduction was greater than what was seen for *S. carnosus-sasG*$_{COL}$ (Figure 6F). β1-4 Galactosidase S reduced the adhesion of both *S. carnosus-sasG*$_{COL}$ and *S. carnosus-sasG*$_{MW2}$ and resulted in a statistically significant reduction for *S. carnosus-sasG*$_{COL}$ (Figure 6G). These data confirm what was observed on corneocytes, that galactose may be important in the structure of a shared ligand between SasG-I and SasG-II, and that β-*N*-acetylglucosamine may be uniquely important to a separate SasG-II ligand structure. Terminal β1-4-linked galactose and β-*N*-acetylglucosamine are found within hybrid N-linked glycans,[34] consistent with our previous observations that Aap binds to *N*-glycans from the glycan array and that PNGase F abrogates adhesion mediated via SasG-I or Aap.[16] However, terminal β1-4-linked galactose and β-*N*-acetylglucosamine are also both found in core 2 mucin-type *O*-glycans.[38] SasG-II may interact with this type of *O*-glycan structure, which would be consistent with the data that SasG-II-mediated adhesion is insensitive to treatment with PNGase F or *O*-glycosidase (*O*-glycosidase can cleave core 1 or core 3, but not core 2 *O*-glycans) (Figure 4).[39] The glycome of healthy skin prominently features numerous N-glycoforms containing lactosamine or sialyllactosamine as well as core 2 *O*-glycans.[35,36]

DISCUSSION

With >50% of bacterial infections becoming resistant to treatment,[40] identifying novel ways to prevent infection has never been more imperative. One of the human body's first defense mechanisms against external hazards is the human skin.[41] *S. aureus* plays an important role in the skin environment, causing the majority of skin and soft tissue infections[5] and

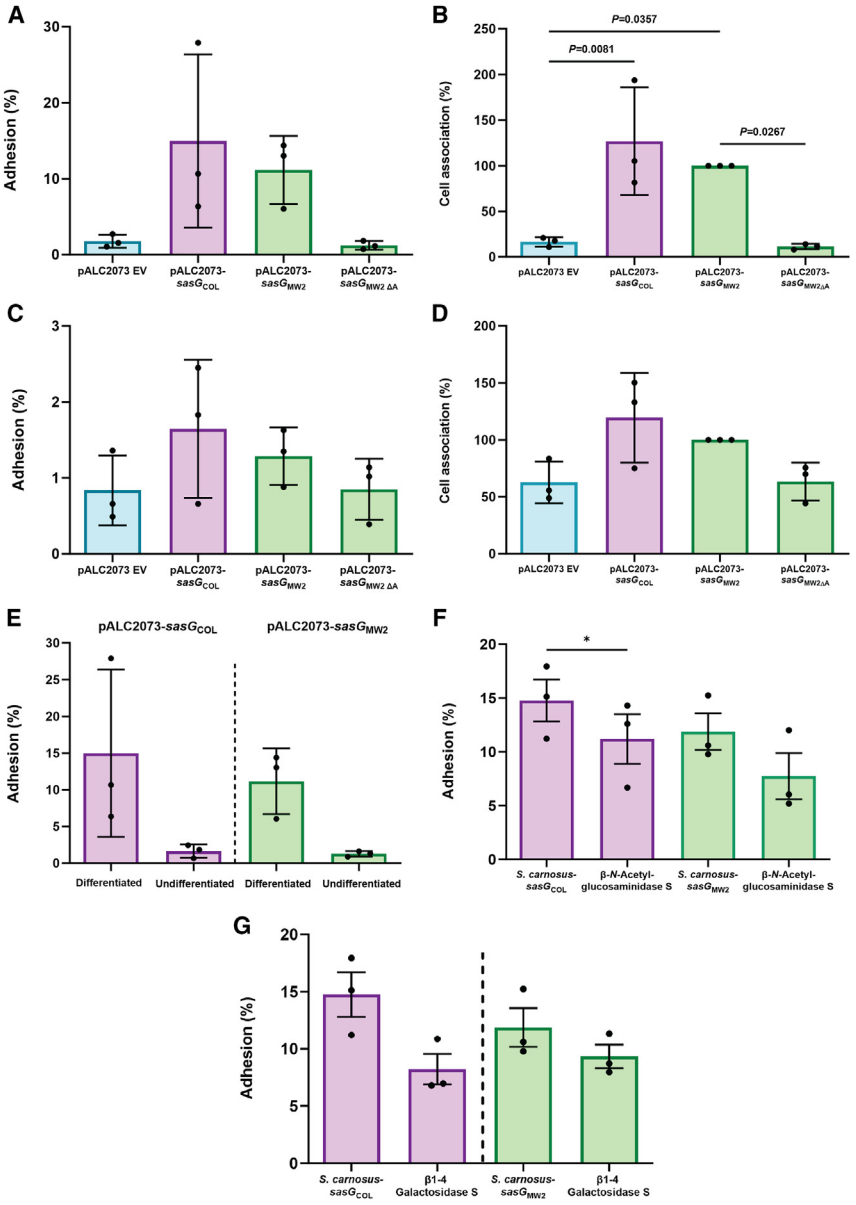

Figure 6. SasG-I- and SasG-II-mediated adhesion to differentiated N/TERT keratinocytes following treatment with glycosidases suggests complex N-linked glycans and core 2 *O*-glycans may be important for SasG-I and SasG-II binding

S. carnosus-pALC2073 EV, SasG-I-expressing *S. carnosus-sasG*$_{COL}$ and SasG-II-expressing *S. carnosus-sasG*$_{MW2}$, and SasG-II-expressing *S. carnosus* with the A domain deleted (*S. carnosus-sasG*$_{MW2\Delta A}$) at an MOI of 5 were tested for adhesion to either differentiated (A and B) or undifferentiated (C and D) N/TERT keratinocytes.

(A) Adhesion to terminally differentiated cells as shown by overall percent adhesion.

(B) Adhesion to terminally differentiated cells as shown by percent cell association to pALC2073-*sasG*$_{MW2}$ input inoculum. Both SasG-expressing strains adhered more to differentiated cells than the EV and A domain mutant controls.

(C) Adhesion to a monolayer of undifferentiated cells as shown by overall percent adhesion.

(D) Adhesion to a monolayer of undifferentiated cells as shown by percent cell association to pALC2073-*sasG*$_{MW2}$ input inoculum. There were no significant differences in adhesion between the EV and A domain mutant controls and the SasG-expressing strains.

(A–D) The colony-forming units (CFU)/mL of 3 independent experiments (n = 3) were calculated and analyzed for statistical significance in GraphPad Prism using ordinary 1-way ANOVA.

(E) Data from (A) and (C) displaying differences in adhesion between differentiated and undifferentiated N/TERT keratinocytes for SasG-I-expressing *S. carnosus-sasG*$_{COL}$ and SasG-II-expressing *S. carnosus-sasG*$_{MW2}$. Both strains adhered well to differentiated N/TERT keratinocytes and did not adhere well to undifferentiated N/TERT keratinocytes. No statistical analyses were performed for (E).

(F and G) SasG-I-expressing *S. carnosus-sasG*$_{COL}$ and SasG-II-expressing *S. carnosus-sasG*$_{MW2}$ were tested for overall percent adhesion to differentiated N/TERT keratinocytes following treatment with (F) β-*N*-acetylglucosaminidase S and (G) β1-4 galactosidase S. β1-4 Galactosidase S reduced adhesion of both strains, whereas β-*N*-acetylglucosaminidase S resulted in a greater reduction in adhesion of *S. carnosus-sasG*$_{MW2}$. The CFU/mL of 3 independent experiments (n = 3) were calculated and analyzed for statistical significance in GraphPad Prism using an unpaired t test. *p = 0.0500.

contributing to morbidity in diseases such as atopic dermatitis.[42–44] Recent studies have emphasized the importance of CWA adhesins in establishing the colonization of human skin corneocytes, which make up the outermost layer of the skin.[13–18] One of these adhesins, SasG, is a multifactorial protein that shares structural and functional similarity to *S. epidermidis* Aap and has been characterized to be important in adhesion to corneocytes from healthy human skin.[15–17] In this study, we identified variation in SasG via phylogenetic analyses, and investigated how this variation affects adhesion to healthy human skin using a multifaceted approach.

Phylogenetic analyses using a curated dataset of the complete genomes from 574 *S. aureus* isolates revealed that approximately one-third of strains express a full-length form and another third express a truncated form of SasG. SasG-I is more than twice as common as SasG-II across the diverse clonal complexes of *S. aureus* examined here. Lastly, approximately one-third of *S. aureus* strains do not encode SasG. Fibronectin-binding protein B was recently found to be important in healthy corneocyte interactions and may explain the ability of *S. aureus* to bind without SasG.[13] SasG-II occurs in some of the earlier diverging clonal complexes, but also occurs in more derived clonal complexes likely due to a historical recombination event; it is unlikely that the two allelic types could independently originate multiple times through mutation alone due to the large number of specific differences that define the two types. The observation that both allelic types of

SasG exist in full-length and truncated forms in currently circulating strains may suggest that retaining this molecular and functional variation is beneficial to *S. aureus* as a species. Thus, SasG may be a candidate for balancing selection in *S. aureus* and needs to be investigated further.[45]

The SasG-II lectin shares 67.2% sequence identity with the SasG-I lectin. Although the overall fold of SasG-II is similar to that of SasG-I and Aap lectin domains, the local architecture in the vicinity of the glycan-binding site differs in SasG-II. In particular, SasG-II lacks the characteristic aromatic residue (Aap Y580 or SasG-I W392) in the floor of the glycan-binding pocket. These aromatic residues in Aap and SasG-I are presumed to form a stacking interaction with a bound glycan ligand, based on the loss of binding for the Y580A and W392A mutants of Aap and SasG-I, respectively.[16] In place of an aromatic residue, the binding pocket in SasG-II features the positively charged R394 residue, which will not allow for a stacking interaction with a bound glycan. Thus, SasG-II may show a loss of glycan specificity compared to Aap and SasG-I. Given their overall sequence and structural similarity, we conjectured that SasG-II may bind the same corneocyte receptor as Aap and SasG-I, but that it may interact with a different or additional glycan ligand(s) not yet identified. Preincubating/blocking healthy human corneocytes with purified lectins from SasG-I and Aap was able to cross-inhibit SasG-II-mediated adhesion to corneocytes, and purified SasG-II was likewise able to cross-inhibit SasG-I and Aap-mediated adhesion. However, unlike the SasG-I and Aap lectins, which were found to bind both *N*-acetyl-D-lactosamine and 3′-sialyl-*N*-acetyllactosamine by Maciag et al.,[16] the SasG-II lectin did not bind *N*-acetyl-D-lactosamine via ITC in our study. This was confirmed via corneocyte adhesion assays, in which this purified glycan did not affect SasG-II-mediated adhesion to corneocytes. This suggests that SasG-II shows specificity for a distinct glycan ligand compared to SasG-I and Aap, but it may bind to the same corneocyte receptor and occlude SasG-I and Aap from binding.

AFM nanoimaging of corneocyte cell surfaces demonstrated weaker and less frequent adhesive interactions for SasG-I than for SasG-II, indicating that although both types strongly bind the ligand present on corneocytes, SasG-II may bind a broader variety of ligands and/or another glycan ligand on corneocytes. In addition, pretreatment of corneocytes with glycosidases resulted in different binding profiles between SasG-I and SasG-II. SasG-I-mediated adhesion was reduced by PNGase F, *O*-glycosidase, α2-3,6,8 neuraminidase, and the exoglycosidases α1-3,4 fucosidase and β1-4 galactosidase S, matching our previous report with the structurally similar *S. epidermidis* Aap.[15] In contrast, SasG-II-mediated adhesion was reduced by only β-*N*-acetylglucosaminidase S and β1-4 galactosidase S. The only glycosidase that resulted in reduced adhesion of both SasG types was β1-4 galactosidase S, suggesting that galactose may be an important terminal sugar residue in a shared ligand between SasG-I and SasG-II, while β-*N*-acetylglucosamine may be important in a ligand unique to SasG-II. Differentiated N/TERT keratinocytes treated with β-*N*-acetylglucosaminidase S and β1-4 galactosidase S further confirmed the corneocyte glycosidase data. Although SasG-I and Aap interact with complex *N*-glycan structures,[16] SasG-II adhesion was unaffected by PNGase F, suggesting that SasG-II may bind to a distinct type of glycan. A likely candidate would be a core 2 *O*-glycan; these can contain terminal β1-4 galactose and β-*N*-acetylglucosamine,[38] but they are insensitive to cleavage by *O*-glycosidase.[39] Interestingly, *N*-glycans containing lactosamine or sialyllactosamine and core 2 *O*-glycans are both prevalent species in the healthy skin glycome.[35,36]

Although we do not know the exact structural nature of the ligand on the corneocyte receptor, our findings strongly suggest that the ligand is expressed on desquamated, terminally differentiated keratinocytes and not basal keratinocytes, both SasG-I and SasG-II are likely to interact with a glycoprotein, and SasG-II may also engage with a core 2 *O*-glycan structure (Figure 7). The findings presented here provide further knowledge that could be used to therapeutically target and prevent *S. aureus* skin colonization for individuals at risk of *S. aureus* infection in a prophylactic manner, potentially eliminating the need for traditional antibiotics that could contribute to further drug resistance in these individuals.

Limitations of the study

A limitation of this study is that the identity of the SasG and Aap ligands and corneocyte receptor have remained elusive, because glycoprotein structures are commonly difficult to solve. This presents a challenge in investigating precise binding properties of and differences between SasG-I and SasG-II, including glycan-binding specificity. The glycan-binding specificity of SasG-I and SasG-II should be investigated further once the specific ligands and corneocyte receptor have been identified.

STAR★METHODS

Detailed methods are provided in the online version of this paper and include the following:

- KEY RESOURCES TABLE
- RESOURCE AVAILABILITY
  - Lead contact
  - Materials availability
  - Data and code availability
- EXPERIMENTAL MODEL AND STUDY PARTICIPANT DETAILS
  - Cell lines
  - Corneocyte collection
  - Microbial strains
- METHOD DETAILS
  - SasG-I and SasG-II lectin alignment
  - SasG phylogenetic analyses
  - SasG-II lectin crystallography
  - Multiparametric imaging using single bacterial probes
  - Isothermal titration calorimetry
  - Corneocyte collection
  - Preparation of bacterial strains for corneocyte and N/TERT adhesion assays
  - Corneocyte adhesion assays
- QUANTIFICATION AND STATISTICAL ANALYSIS

SUPPLEMENTAL INFORMATION

Supplemental information can be found online at https://doi.org/10.1016/j.celrep.2024.114022.

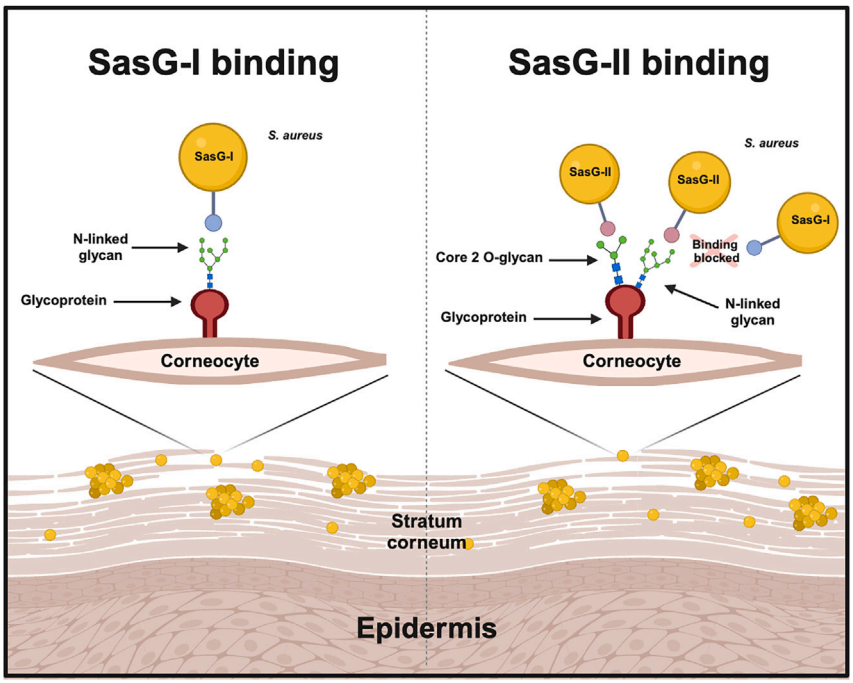

Figure 7. Model for SasG-I- and SasG-II-mediated adhesion to healthy human skin corneocytes

SasG-I blocks adhesion of SasG-II, and likewise SasG-II can block adhesion of SasG-I, indicating that they can bind the same corneocyte receptor in some capacity. Since SasG-II does not bind *N*-acetyllactosamine in the same manner as SasG-I, we predict that SasG-II may block SasG-I sterically, perhaps through binding to a region of the receptor adjacent to the *N*-glycan. In addition, the removal of *N*-glycans and core 1 or 3 *O*-glycans does not block SasG-II binding as it does with SasG-I, suggesting that SasG-II may bind a core 2 *O*-glycan structure elsewhere on the corneocyte receptor. This figure was created in BioRender.com.

ACKNOWLEDGMENTS

This work was funded by NIH/NIAID grant AI162964 to A.R.H., A.B.H., and P.D.F. and GM094363 to A.B.H. Work at UCLouvain was supported by the National Fund for Scientific Research (FNRS). Y.F.D. is a research director at the FNRS. This research used resources of the Advanced Photon Source, a US Department of Energy (DOE) Office of Science User Facility operated for the DOE Office of Science by Argonne National Laboratory under contract no. DE-AC02-06CH11357. SasG-II diffraction data were collected at the Northeastern Collaborative Access Team (NE-CAT) beamline 24-ID-E, which is funded by the NIH through NIGMS (P30 GM124165). The Eiger 16M detector on 24-ID-E is funded by a NIH-ORIP HEI grant (S10OD021527).

AUTHOR CONTRIBUTIONS

Data development, manuscript writing, intellectual development, and presentations of the published work were contributed by K.B.M. Data development, intellectual development, and/or methods were contributed by J.J.M., C.W., J.A.C., T.J.E., K.C.K., Y.F.D., and D.A.R. Manuscript editing, funding, project oversight, and intellectual development were contributed by P.D.F., A.B.H., and A.R.H.

DECLARATION OF INTERESTS

A.B.H. has served as a scientific advisory board member for Hoth Therapeutics, holds equity in Hoth Therapeutics and Chelexa BioSciences, and was a co-inventor on seven patents broadly related to the subject matter of this work.

Received: August 30, 2023
Revised: January 23, 2024
Accepted: March 15, 2024
Published: April 2, 2024

REFERENCES

1. Parlet, C.P., Brown, M.M., and Horswill, A.R. (2019). Commensal Staphylococci Influence Staphylococcus aureus Skin Colonization and Disease. Trends Microbiol. *27*, 497–507. https://doi.org/10.1016/j.tim.2019.01.008.
2. Brown, A.F., Leech, J.M., Rogers, T.R., and McLoughlin, R.M. (2014). Staphylococcus aureus Colonization: Modulation of Host Immune Response and Impact on Human Vaccine Design. Front. Immunol. *4*, 507. https://doi.org/10.3389/fimmu.2013.00507.
3. Otto, M. (2010). Staphylococcus colonization of the skin and antimicrobial peptides. Expet Rev. Dermatol. *5*, 183–195. https://doi.org/10.1586/edm.10.6.
4. von Eiff, C., Becker, K., Machka, K., Stammer, H., and Peters, G. (2001). Nasal carriage as a source of Staphylococcus aureus bacteremia. Study Group. N. Engl. J. Med. *344*, 11–16. https://doi.org/10.1056/NEJM200101043440102.
5. Moran, G.J., Krishnadasan, A., Gorwitz, R.J., Fosheim, G.E., McDougal, L.K., Carey, R.B., and Talan, D.A.; EMERGEncy ID Net Study Group (2006). Methicillin-resistant S. aureus infections among patients in the emergency department. N. Engl. J. Med. *355*, 666–674. https://doi.org/10.1056/NEJMoa055356.
6. Leung, D.Y.M. (2003). Infection in atopic dermatitis. Curr. Opin. Pediatr. *15*, 399–404. https://doi.org/10.1097/00008480-200308000-00008.
7. Bieber, T. (2020). Targeting T2 Inflammation by Dupilumab Impacts on the Microbiomic "Menage a Trois" of Atopic Dermatitis. J. Invest. Dermatol. *140*, 15–17. https://doi.org/10.1016/j.jid.2019.07.680.
8. Brown, M.M., Kwiecinski, J.M., Cruz, L.M., Shahbandi, A., Todd, D.A., Cech, N.B., and Horswill, A.R. (2020). Novel Peptide from Commensal Staphylococcus simulans Blocks Methicillin-Resistant Staphylococcus aureus Quorum Sensing and Protects Host Skin from Damage. Antimicrob. Agents Chemother. *64*, e00172-20. https://doi.org/10.1128/AAC.00172-20.
9. Lee, S.M., Keum, H.L., and Sul, W.J. (2023). Bacterial Crosstalk via Antimicrobial Peptides on the Human Skin: Therapeutics from a Sustainable Perspective. J. Microbiol. *61*, 1–11. https://doi.org/10.1007/s12275-022-00002-8.
10. Burian, M., Wolz, C., and Yazdi, A.S. (2022). Transcriptional adaptation of staphylococci during colonization of the authentic human environment: An overview of transcriptomic changes and their relationship to physiological conditions. Front. Cell. Infect. Microbiol. *12*, 1062329. https://doi.org/10.3389/fcimb.2022.1062329.

11. Foster, T.J., Geoghegan, J.A., Ganesh, V.K., and Höök, M. (2014). Adhesion, invasion and evasion: the many functions of the surface proteins of Staphylococcus aureus. Nat. Rev. Microbiol. *12*, 49–62. https://doi.org/10.1038/nrmicro3161.

12. Nakatsuji, T., Chen, T.H., Two, A.M., Chun, K.A., Narala, S., Geha, R.S., Hata, T.R., and Gallo, R.L. (2016). Staphylococcus aureus Exploits Epidermal Barrier Defects in Atopic Dermatitis to Trigger Cytokine Expression. J. Invest. Dermatol. *136*, 2192–2200. https://doi.org/10.1016/j.jid.2016.05.127.

13. da Costa, T.M., Viljoen, A., Towell, A.M., Dufrêne, Y.F., and Geoghegan, J.A. (2022). Fibronectin binding protein B binds to loricrin and promotes corneocyte adhesion by Staphylococcus aureus. Nat. Commun. *13*, 2517. https://doi.org/10.1038/s41467-022-30271-1.

14. Fleury, O.M., McAleer, M.A., Feuillie, C., Formosa-Dague, C., Sansevere, E., Bennett, D.E., Towell, A.M., McLean, W.H.I., Kezic, S., Robinson, D.A., et al. (2017). Clumping Factor B Promotes Adherence of Staphylococcus aureus to Corneocytes in Atopic Dermatitis. Infect. Immun. *85*, e00994-16. https://doi.org/10.1128/IAI.00994-16.

15. Roy, P., Horswill, A.R., and Fey, P.D. (2021). Glycan-Dependent Corneocyte Adherence of Staphylococcus epidermidis Mediated by the Lectin Subdomain of Aap. mBio *12*, e0290820. https://doi.org/10.1128/mBio.02908-20.

16. Maciag, J.J., Chantraine, C., Mills, K.B., Yadav, R., Yarawsky, A.E., Chaton, C.T., Vinod, D., Fitzkee, N.C., Mathelié-Guinlet, M., Dufrêne, Y.F., et al. (2023). Mechanistic basis of staphylococcal interspecies competition for skin colonization. Preprint at bioRxiv. https://doi.org/10.1101/2023.01.26.525635.

17. Mills, K.B., Roy, P., Kwiecinski, J.M., Fey, P.D., and Horswill, A.R. (2022). Staphylococcal Corneocyte Adhesion: Assay Optimization and Roles of Aap and SasG Adhesins in the Establishment of Healthy Skin Colonization. Microbiol. Spectr. *10*, e0246922. https://doi.org/10.1128/spectrum.02469-22.

18. Corrigan, R.M., Rigby, D., Handley, P., and Foster, T.J. (2007). The role of Staphylococcus aureus surface protein SasG in adherence and biofilm formation. Microbiology (Read.) *153*, 2435–2446. https://doi.org/10.1099/mic.0.2007/006676-0.

19. Crosby, H.A., Schlievert, P.M., Merriman, J.A., King, J.M., Salgado-Pabón, W., and Horswill, A.R. (2016). The Staphylococcus aureus Global Regulator MgrA Modulates Clumping and Virulence by Controlling Surface Protein Expression. PLoS Pathog. *12*, e1005604. https://doi.org/10.1371/journal.ppat.1005604.

20. Yarawsky, A.E., Ori, A.L., English, L.R., Whitten, S.T., and Herr, A.B. (2023). Convergent behavior of extended stalk regions from staphylococcal surface proteins with widely divergent sequence patterns. Protein Sci. *32*, e4707. https://doi.org/10.1002/pro.4707.

21. Cummings, R.D., E., M.E., Ramya, T.N.C., Kato, K., Rabinovich, G.A., and Surolia, A. (2022). L-Type Lectins. In Essentials of Glycobiology, A. Varki, R.D. Cummings, J.D. Esko, P. Stanley, G.W. Hart, M. Aebi, D. Mohnen, T. Kinoshita, N.H. Packer, and J.H. Prestegard, et al., eds.. https://doi.org/10.1101/9781621824213.

22. Severn, M.M., and Horswill, A.R. (2023). Staphylococcus epidermidis and its dual lifestyle in skin health and infection. Nat. Rev. Microbiol. *21*, 97–111. https://doi.org/10.1038/s41579-022-00780-3.

23. Tolo, I., Thomas, J.C., Fischer, R.S.B., Brown, E.L., Gray, B.M., and Robinson, D.A. (2016). Do Staphylococcus epidermidis Genetic Clusters Predict Isolation Sources? J. Clin. Microbiol. *54*, 1711–1719. https://doi.org/10.1128/JCM.03345-15.

24. McCarthy, A.J., and Lindsay, J.A. (2010). Genetic variation in Staphylococcus aureus surface and immune evasion genes is lineage associated: implications for vaccine design and host-pathogen interactions. BMC Microbiol. *10*, 173. https://doi.org/10.1186/1471-2180-10-173.

25. Geoghegan, J.A., Corrigan, R.M., Gruszka, D.T., Speziale, P., O'Gara, J.P., Potts, J.R., and Foster, T.J. (2010). Role of surface protein SasG in biofilm formation by Staphylococcus aureus. J. Bacteriol. *192*, 5663–5673. https://doi.org/10.1128/JB.00628-10.

26. Kuroda, M., Ohta, T., Uchiyama, I., Baba, T., Yuzawa, H., Kobayashi, I., Cui, L., Oguchi, A., Aoki, K., Nagai, Y., et al. (2001). Whole genome sequencing of meticillin-resistant Staphylococcus aureus. Lancet *357*, 1225–1240. https://doi.org/10.1016/s0140-6736(00)04403-2.

27. Bonn, C.M., Rafiqullah, I.M., Crawford, J.A., Qian, Y.M., Guthrie, J.L., Matuszewska, M., Robinson, D.A., and McGavin, M.J. (2023). Repeated Emergence of Variant TetR Family Regulator, FarR, and Increased Resistance to Antimicrobial Unsaturated Fatty Acid among Clonal Complex 5 Methicillin-Resistant Staphylococcus aureus. Antimicrob. Agents Chemother. *67*, e0074922. https://doi.org/10.1128/aac.00749-22.

28. Challagundla, L., Reyes, J., Rafiqullah, I., Sordelli, D.O., Echaniz-Aviles, G., Velazquez-Meza, M.E., Castillo-Ramírez, S., Fittipaldi, N., Feldgarden, M., Chapman, S.B., et al. (2018). Phylogenomic Classification and the Evolution of Clonal Complex 5 Methicillin-Resistant Staphylococcus aureus in the Western Hemisphere. Front. Microbiol. *9*, 1901. https://doi.org/10.3389/fmicb.2018.01901.

29. Dabul, A.N.G., and Camargo, I.L.B.C. (2014). Clonal complexes of Staphylococcus aureus: all mixed and together. FEMS Microbiol. Lett. *351*, 7–8. https://doi.org/10.1111/1574-6968.12358.

30. Bowers, J.R., Driebe, E.M., Albrecht, V., McDougal, L.K., Granade, M., Roe, C.C., Lemmer, D., Rasheed, J.K., Engelthaler, D.M., Keim, P., and Limbago, B.M. (2018). Improved Subtyping of Staphylococcus aureus Clonal Complex 8 Strains Based on Whole-Genome Phylogenetic Analysis. mSphere *3*, e00464-17. https://doi.org/10.1128/mSphere.00464-17.

31. Clark, L.C., Atkin, K.E., Whelan, F., Brentnall, A.S., Harris, G., Towell, A.M., Turkenburg, J.P., Liu, Y., Feizi, T., Griffiths, S.C., et al. (2023). Staphylococcal Periscope proteins Aap, SasG, and Pls project noncanonical legume-like lectin adhesin domains from the bacterial surface. J. Biol. Chem. *299*, 102936. https://doi.org/10.1016/j.jbc.2023.102936.

32. Dufrêne, Y.F., Ando, T., Garcia, R., Alsteens, D., Martinez-Martin, D., Engel, A., Gerber, C., and Müller, D.J. (2017). Imaging modes of atomic force microscopy for application in molecular and cell biology. Nat. Nanotechnol. *12*, 295–307. https://doi.org/10.1038/nnano.2017.45.

33. Abdayem, R., Formanek, F., Minondo, A.M., Potter, A., and Haftek, M. (2016). Cell surface glycans in the human stratum corneum: distribution and depth-related changes. Exp. Dermatol. *25*, 865–871. https://doi.org/10.1111/exd.13070.

34. Danzberger, J., Donovan, M., Rankl, C., Zhu, R., Vicic, S., Baltenneck, C., Enea, R., Hinterdorfer, P., and Luengo, G.S. (2018). Glycan distribution and density in native skin's stratum corneum. Skin Res. Technol. *24*, 450–458. https://doi.org/10.1111/srt.12453.

35. Dabelsteen, S., Pallesen, E.M.H., Marinova, I.N., Nielsen, M.I., Adamopoulou, M., Rømer, T.B., Levann, A., Andersen, M.M., Ye, Z., Thein, D., et al. (2020). Essential Functions of Glycans in Human Epithelia Dissected by a CRISPR-Cas9-Engineered Human Organotypic Skin Model. Dev. Cell *54*, 669–684.e7. https://doi.org/10.1016/j.devcel.2020.06.039.

36. Möginger, U., Grunewald, S., Hennig, R., Kuo, C.W., Schirmeister, F., Voth, H., Rapp, E., Khoo, K.H., Seeberger, P.H., Simon, J.C., and Kolarich, D. (2018). Alterations of the Human Skin N- and O-Glycome in Basal Cell Carcinoma and Squamous Cell Carcinoma. Front. Oncol. *8*, 70. https://doi.org/10.3389/fonc.2018.00070.

37. Tang, L., Chen, X., Zhang, X., Guo, Y., Su, J., Zhang, J., Peng, C., and Chen, X. (2019). N-Glycosylation in progression of skin cancer. Med. Oncol. *36*, 50. https://doi.org/10.1007/s12032-019-1270-4.

38. Beckwith, D.M., and Cudic, M. (2020). Tumor-associated O-glycans of MUC1: Carriers of the glyco-code and targets for cancer vaccine design. Semin. Immunol. *47*, 101389. https://doi.org/10.1016/j.smim.2020.101389.

39. Koutsioulis, D., Landry, D., and Guthrie, E.P. (2008). Novel endo-alpha-N-acetylgalactosaminidases with broader substrate specificity. Glycobiology *18*, 799–805. https://doi.org/10.1093/glycob/cwn069.

40. WHO (2022). Report Signals Increasing Resistance to Antibiotics in Bacterial Infections in Humans and Need for Better Data. https://www.who.int/news/item/09-12-2022-report-signals-increasing-resistance-to-antibiotics-in-bacterial-infections-in-humans-and-need-for-better-data#:~:text=A%20new%20World%20Health%20Organization,by%2087%20countries%20in%202020.
41. Eyerich, S., Eyerich, K., Traidl-Hoffmann, C., and Biedermann, T. (2018). Cutaneous Barriers and Skin Immunity: Differentiating A Connected Network. Trends Immunol. *39*, 315–327. https://doi.org/10.1016/j.it.2018.02.004.
42. Ogonowska, P., Gilaberte, Y., Barańska-Rybak, W., and Nakonieczna, J. (2020). Colonization With Staphylococcus aureus in Atopic Dermatitis Patients: Attempts to Reveal the Unknown. Front. Microbiol. *11*, 567090. https://doi.org/10.3389/fmicb.2020.567090.
43. Silverberg, J.I. (2017). Public Health Burden and Epidemiology of Atopic Dermatitis. Dermatol. Clin. *35*, 283–289. https://doi.org/10.1016/j.det.2017.02.002.
44. Avena-Woods, C. (2017). Overview of Atopic Dermatitis. Am. J. Manag. Care *23*, S115–S123.
45. Thomas, J.C., Godfrey, P.A., Feldgarden, M., and Robinson, D.A. (2012). Candidate targets of balancing selection in the genome of Staphylococcus aureus. Mol. Biol. Evol. *29*, 1175–1186. https://doi.org/10.1093/molbev/msr286.
46. Smits, J.P.H., Niehues, H., Rikken, G., van Vlijmen-Willems, I.M.J.J., van de Zande, G.W.H.J.F., Zeeuwen, P.L.J.M., Schalkwijk, J., and van den Bogaard, E.H. (2017). Immortalized N/TERT keratinocytes as an alternative cell source in 3D human epidermal models. Sci. Rep. *7*, 11838. https://doi.org/10.1038/s41598-017-12041-y.
47. Sievers, F., Wilm, A., Dineen, D., Gibson, T.J., Karplus, K., Li, W., Lopez, R., McWilliam, H., Remmert, M., Söding, J., et al. (2011). Fast, scalable generation of high-quality protein multiple sequence alignments using Clustal Omega. Mol. Syst. Biol. *7*, 539. https://doi.org/10.1038/msb.2011.75.
48. Robert, X., and Gouet, P. (2014). Deciphering key features in protein structures with the new ENDscript server. Nucleic Acids Res. *42*, W320–W324. https://doi.org/10.1093/nar/gku316.
49. Snyder, E.E., Kampanya, N., Lu, J., Nordberg, E.K., Karur, H.R., Shukla, M., Soneja, J., Tian, Y., Xue, T., Yoo, H., et al. (2007). PATRIC: the VBI PathoSystems Resource Integration Center. Nucleic Acids Res. *35*, D401–D406. https://doi.org/10.1093/nar/gkl858.
50. Wattam, A.R., Abraham, D., Dalay, O., Disz, T.L., Driscoll, T., Gabbard, J.L., Gillespie, J.J., Gough, R., Hix, D., Kenyon, R., et al. (2014). PATRIC, the bacterial bioinformatics database and analysis resource. Nucleic Acids Res. *42*, D581–D591. https://doi.org/10.1093/nar/gkt1099.
51. Wattam, A.R., Davis, J.J., Assaf, R., Boisvert, S., Brettin, T., Bun, C., Conrad, N., Dietrich, E.M., Disz, T., Gabbard, J.L., et al. (2017). Improvements to PATRIC, the all-bacterial Bioinformatics Database and Analysis Resource Center. Nucleic Acids Res. *45*, D535–D542. https://doi.org/10.1093/nar/gkw1017.
52. Asnicar, F., Thomas, A.M., Beghini, F., Mengoni, C., Manara, S., Manghi, P., Zhu, Q., Bolzan, M., Cumbo, F., May, U., et al. (2020). Precise phylogenetic analysis of microbial isolates and genomes from metagenomes using PhyloPhlAn 3.0. Nat. Commun. *11*, 2500. https://doi.org/10.1038/s41467-020-16366-7.
53. Edgar, R.C. (2004). MUSCLE: multiple sequence alignment with high accuracy and high throughput. Nucleic Acids Res. *32*, 1792–1797. https://doi.org/10.1093/nar/gkh340.
54. Edgar, R.C. (2004). MUSCLE: a multiple sequence alignment method with reduced time and space complexity. BMC Bioinf. *5*, 113. https://doi.org/10.1186/1471-2105-5-113.
55. Fu, L., Niu, B., Zhu, Z., Wu, S., and Li, W. (2012). CD-HIT: accelerated for clustering the next-generation sequencing data. Bioinformatics *28*, 3150–3152. https://doi.org/10.1093/bioinformatics/bts565.
56. Huang, Y., Niu, B., Gao, Y., Fu, L., and Li, W. (2010). CD-HIT Suite: a web server for clustering and comparing biological sequences. Bioinformatics *26*, 680–682. https://doi.org/10.1093/bioinformatics/btq003.
57. Talavera, G., and Castresana, J. (2007). Improvement of phylogenies after removing divergent and ambiguously aligned blocks from protein sequence alignments. Syst. Biol. *56*, 564–577. https://doi.org/10.1080/10635150701472164.
58. Guindon, S., Dufayard, J.F., Lefort, V., Anisimova, M., Hordijk, W., and Gascuel, O. (2010). New algorithms and methods to estimate maximum-likelihood phylogenies: assessing the performance of PhyML 3.0. Syst. Biol. *59*, 307–321. https://doi.org/10.1093/sysbio/syq010.
59. Maddison, W.P., and Maddison, D.R. (2021). Mesquite: A Modular System for Evolutionary Analysis. http://www.mesquiteproject.org.
60. Winn, M.D., Ballard, C.C., Cowtan, K.D., Dodson, E.J., Emsley, P., Evans, P.R., Keegan, R.M., Krissinel, E.B., Leslie, A.G.W., McCoy, A., et al. (2011). Overview of the CCP4 suite and current developments. Acta Crystallogr. D Biol. Crystallogr. *67*, 235–242. https://doi.org/10.1107/S0907444910045749.
61. Liebschner, D., Afonine, P.V., Baker, M.L., Bunkóczi, G., Chen, V.B., Croll, T.I., Hintze, B., Hung, L.W., Jain, S., McCoy, A.J., et al. (2019). Macromolecular structure determination using X-rays, neutrons and electrons: recent developments in Phenix. Acta Crystallogr. D Struct. Biol. *75*, 861–877. https://doi.org/10.1107/S2059798319011471.
62. Emsley, P., Lohkamp, B., Scott, W.G., and Cowtan, K. (2010). Features and development of Coot. Acta Crystallogr. D Biol. Crystallogr. *66*, 486–501. https://doi.org/10.1107/S0907444910007493.
63. Chen, V.B., Arendall, W.B., 3rd, Headd, J.J., Keedy, D.A., Immormino, R.M., Kapral, G.J., Murray, L.W., Richardson, J.S., and Richardson, D.C. (2010). MolProbity: all-atom structure validation for macromolecular crystallography. Acta Crystallogr. D Biol. Crystallogr. *66*, 12–21. https://doi.org/10.1107/S0907444909042073.
64. Wang, C., Chantraine, C., Viljoen, A., Herr, A.B., Fey, P.D., Horswill, A.R., Mathelié-Guinlet, M., and Dufrêne, Y.F. (2022). The staphylococcal biofilm protein Aap mediates cell-cell adhesion through mechanically distinct homophilic and lectin interactions. PNAS Nexus *1*, pgac278. https://doi.org/10.1093/pnasnexus/pgac278.
65. Bechhoefer, J.L.H.a.J. (1993). Calibration of atomic-force microscope tips. Rev. Sci. Instrum., 1868–1873. https://doi.org/10.1063/1.1143970.

STAR★METHODS

KEY RESOURCES TABLE

REAGENT or RESOURCE	SOURCE	IDENTIFIER
Bacterial and virus strains		
E. coli BLR (DE3)	Novagen	N/A
S. epidermidis Δ*ica* + pCM29	Dr. Paul D Fey	AH2983
S. epidermidis Δ*ica* Δ*aap* + pCM29	Dr. Paul D Fey	AH2984
MRSA Δ*mgrA* + pCM29	Dr. Alexander R Horswill	AH4478
MRSA Δ*mgrA* Δ*sasG* + pCM29	Dr. Alexander R Horswill (this paper)	AH4834
S. carnosus Δ*SCA_2238*::sGFP Δ*SCA_2092* + pALC2073-*sasG*$_{MW2}$	Dr. Alexander R Horswill	AH5905
S. carnosus Δ*SCA_2238*::sGFP Δ*SCA_2092* + pALC2073	Dr. Alexander R Horswill	AH5907
S. carnosus Δ*SCA 2238*::sGFP Δ*SCA_2092* + pALC2073-*sasG*$_{COL}$	Dr. Alexander R Horswill	AH5908
S. carnosus Δ*SCA_2238*::sGFP Δ*SCA_2092* + pHC109 (pALC2073-*sasG*$_{MW2ΔA}$)	Dr. Alexander R Horswill	AH6012
Biological samples		
Human desquamated corneocytes	University of Colorado Anschutz Medical Campus; Dr. Joan Geoghegan (this paper)	N/A
Chemicals, peptides, and recombinant proteins		
Aap recombinant lectin	Dr. Andrew B Herr	N/A
Aap ΔY580A recombinant lectin	Dr. Andrew B Herr	N/A
SasG-I recombinant lectin	Dr. Andrew B Herr	N/A
SasG-I ΔW392A recombinant lectin	Dr. Andrew B Herr	N/A
SasG-II recombinant lectin	Dr. Andrew B Herr (this paper)	N/A
SasG-II full-length recombinant protein	Dr. Alexander R Horswill	N/A
SasG-II A-domain recombinant protein	Dr. Alexander R Horswill (this paper)	N/A
N-acetyl-D-lactosamine	Sigma-Aldrich	Cat# 32181-59-2
3′-sialyl-*N*-acetyllactosamine	Sigma-Aldrich	Cat# 102490-37-9
PNGase F	New England Biolabs	Cat# P0704S
O-Glycosidase	New England Biolabs	Cat# E0540S
α1-2,3,6 Mannosidase	New England Biolabs	Cat# P0768S
α1-3,4 Fucosidase	New England Biolabs	Cat# P0769S
β-N-Acetylglucosaminidase S	New England Biolabs	Cat# P0744S
β1-4 Galactosidase S	New England Biolabs	Cat# P0745S
α2-3,6,8 Neuraminidase	New England Biolabs	Cat# E0540S
Deposited data		
SasG-II lectin coordinates	RCSB Protein DataBank	PDB code: 8TB2
Experimental models: Cell lines		
Immortalized N/TERT-2G keratinocytes	Dr. James Rheinwald	N/A
Recombinant DNA		
pDest17-His	Thermo Fisher	Cat# 11803012
pALC2073-*sasG*$_{MW2}$	Dr. Alexander R Horswill	N/A
pALC2073-*sasG*$_{COL}$	Dr. Alexander R Horswill	N/A
pHC109	Dr. Alexander R Horswill	N/A

(*Continued on next page*)

Continued

REAGENT or RESOURCE	SOURCE	IDENTIFIER
Software and algorithms		
Clustal Omega 1.2.4	http://www.ebi.ac.uk/Tools/msa/clustalo/	RRID:SCR_001591
ESPript 3.0	http://espript.ibcp.fr/ESPript/ESPript/	RRID:SCR_006587
PhyloPhlAn3	https://bitbucket.org/nsegata/phylophlan/wiki/Home	RRID:SCR_013082
MUSCLE v3.8.31	http://www.ebi.ac.uk/Tools/msa/muscle/	RRID:SCR_011812
CD-HIT v4.8.1	http://weizhong-lab.ucsd.edu/cd-hit/(no longer in service)	RRID:SCR_007105
Gblocks v0.91b	http://molevol.cmima.csic.es/castresana/Gblocks_server.html	RRID:SCR_015945
PhyML	http://www.atgc-montpellier.fr/phyml/	RRID:SCR_014629
Mesquite v3.70	https://www.mesquiteproject.org/	RRID:SCR_017994
R statistics package	http://www.r-project.org/	RRID:SCR_001905
GraphPad Prism	http://www.graphpad.com/	RRID:SCR_002798
CCP4i suite	http://www.ccp4.ac.uk/	RRID:SCR_007255
PHENIX: PHASER	https://www.phenix-online.org/documentation/reference/phaser.html	RRID:SCR_014219
PHENIX	https://www.phenix-online.org/	RRID:SCR_014224
Coot	http://www2.mrc-lmb.cam.ac.uk/personal/pemsley/coot/	RRID:SCR_014222
MolProbity	http://molprobity.biochem.duke.edu	RRID:SCR_014226
ORIGIN	http://www.originlab.com/index.aspx?go=PRODUCTS/Origin	RRID:SCR_014212
FIJI - ImageJ	https://imagej.net/software/fiji/	RRID:SCR_002285
Other		
BZ-X710 microscope	Keyence	N/A
Nanowizard III and IV AFM	JPK Instruments	N/A

RESOURCE AVAILABILITY

Lead contact

Further information and requests for resources and reagents should be directed to and will be fulfilled by the lead contact, Alexander R. Horswill (alexander.horswill@cuanschutz.edu).

Materials availability

Protein coordinates generated in this study have been deposited to the RCSB with PDB code 8TB2.

Data and code availability

- All data reported in this paper will be shared by the lead contact upon request.
- This paper does not report original code.
- Any additional information required to reanalyze the data reported in this work paper is available from the lead contact upon request.

EXPERIMENTAL MODEL AND STUDY PARTICIPANT DETAILS

Cell lines

Low passage (<10), undifferentiated, immortalized N/TERT-2G cells were seeded to $1x10^5$ cells/mL in either experiment media (EM)[46] or keratinocyte serum-free medium (KSFM, Gibco) in a 24-well tissue culture treated plate. For the assays on differentiated N/TERT-2G cells, the keratinocytes were both seeded in and allowed to differentiate in EM for 1 week with media changes every two days to promote the formation of a stratified and thick layer of epithelial cells. For assays using undifferentiated N/TERT-2G cells, cells were seeded in KSFM and were allowed to form a 100% confluent monolayer (approximately 2–3 days growth) with daily media changes. All cells were grown at 37°C with 5% CO_2.

Corneocyte collection

Desquamated corneocytes from the lower or upper arm near the elbow were collected from healthy human volunteers of both sexes and used directly for experiments.[17] No institutional protocol was needed.

Microbial strains

Microbial strains used in this study are listed in Table S2. The day before experimentation, strains were grown overnight at 37°C with shaking aeration at 220 rpm in tryptic soy broth (TSB) in the presence of 10 μg/mL of chloramphenicol for plasmid maintenance. Experiments were approved by the institutional biosafety committee under protocol number IBC-00001264.

METHOD DETAILS

SasG-I and SasG-II lectin alignment

The lectin protein sequences of SasG-I (from MSSA 502a) and SasG-II (from MRSA MW2) were aligned using Clustal Omega 1.2.4.[47] Sequence similarities, secondary structure elements, and relative accessibility were extracted with the Clustal Omega protein alignment and Type I/Type II lectin protein coordinates using the DSSP program in ESPript 3.0.[48]

SasG phylogenetic analyses

Variation in SasG was analyzed in the context of *S. aureus* phylogenetic diversity. In brief, a previously curated dataset of complete genomes from 574 *S aureus* isolates, and 1 *S argenteus* isolate that served as an outgroup, was obtained from the PATRIC database.[49–51] PhyloPhlAn3[52] was used to align conceptually translated protein sequences from the *S. aureus* proteome, curate the alignment, and perform phylogenetic analysis using default settings. Clonal complexes were identified on the phylogeny as clusters of related multilocus sequence types. SasG sequences were extracted from these proteomes and strains were sorted into three groups based on the state of their SasG sequence as full-length, truncated, or absent. Full-length SasG sequences were aligned with MUSCLE v3.8.31[53,54] and clustered with CD-HIT v4.8.1[55,56] at 100% identity. Gblocks v0.91b[57] was used with stringent settings (min. seq. for flank pos.: 85%, max. contig. nonconserved pos.: 4, min. block length: 10, no gaps in final blocks) to remove alignment gaps, including the SasG B-repeat sequences. PhyML[58] was used with the WAG model to infer a SasG phylogeny and to define two SasG allelic types. Mesquite v3.70[59] was used to perform parsimony analysis with the *S. aureus* phylogeny to reconstruct SasG presence/absence and SasG allelic type; since the parsimony analysis ignores branch lengths it was not necessary to account for recombination events on the *S. aureus* phylogeny for this analysis. The R statistics package was used to perform a chi-squared goodness-of-fit test of the B-repeat distributions of the two SasG allelic types.

SasG-II lectin crystallography

The SasG-II lectin domain was expressed as a fusion protein with an N-terminal hexahistidine tag followed by a tobacco etch virus (TEV) protease site using the pDest17-His plasmid in *E. coli* BLR (DE3) cells (Novagen). Protein expression and purification were conducted as described for the SasG-I lectin domain.[16] Crystals were grown via hanging drop diffusion. Protein stocks were at a concentration of 10 mg/mL in 20 mM Tris-HCl (pH 7.2) and 300 mM NaCl. Stocks were combined with mother liquor in equal parts (1 μL + 1 μL). Crystals appeared after five days in a condition of 100 mM HEPES (pH 7.8), 200 mM Ammonium Sulfate, 25%–33% BCS PEG SMEAR Medium (Molecular Dimensions, CalibreScientific). Cryoprotectant consisted of 80% mother liquor and 20% MPD; crystals were plunged into cryoprotectant prior to being flash frozen in liquid nitrogen. Data collection occurred at the Advanced Photon Source at Argonne National Lab through the Northeastern Collaborative Access Team (NE-CAT) on the 24-ID-E beamline. Datasets were collected at an oscillation range of 0.2°, collecting 900 frames, at a resolution range of 78.074–1.799 Å. Data indexing, space group assignment, scaling, and integration were carried out in the CCP4i suite.[60] Structure determination was carried out by PHENIX: PHASER using Aap lectin[16] as a search model for molecular replacement and building the initial SasG-II model with PHENIX: Autobuild. Iterative cycles of refinement and model building using data to a maximum resolution of 1.88 Å were carried out using PHENIX[61] and Coot,[62] respectively. The final refined model was submitted for validation using MolProbity.[63]

Multiparametric imaging using single bacterial probes

SasG-I-expressing *S. carnosus*-SasG$_{COL}$, SasG-II-expressing *S. carnosus-sasG*$_{MW2}$, or *S. carnosus*-pALC2073 (EV) and a healthy skin corneocyte (0.5 cm × 0.5 cm) were immobilized on two different and separate areas on the bottom of a Petri dish. The corneocyte was attached to one side of the Petri dish using a double-sided transparent tape. 50 μL of diluted bacterial suspension in phosphate-buffered saline (PBS) was deposited on the other side of a Petri dish and allowed to adhere for 15 min at room temperature. The Petri dish was then carefully washed twice with PBS to remove non-adhering cells, after which 3 mL of PBS buffer was added to perform atomic force microscopy (AFM) experiments.

Single-cell probes were obtained by attaching a single bacterium to a colloidal probe. Colloidal probes were prepared as elucidated previously.[64] Colloidal probe cantilevers were immersed for 60 min in Tris-buffered saline (TBS; Tris, 50 mM; NaCl, 150 mM; pH 8.5) containing 4 mg mL^{-1} of dopamine hydrochloride (Sigma-Aldrich), rinsed in TBS, and used directly for cell probe preparation. The nominal spring constant of the colloidal probe cantilever was determined by the thermal noise method,[65] giving an average value of ~0.06 N/m. The colloidal probe was brought into contact with a single isolated bacterium to catch it via electrostatic

interaction with polydopamine and then moved on top of the corneocyte (kindly provided by Prof. Joan Geoghegan); proper attachment of the cell on the colloidal probe was checked using optical microscopy.

Multiparametric images of corneocytes were recorded in PBS using a bacterial probe under the Quantitative Imaging mode available on the Nanowizard III and IV AFM (JPK Instruments, Germany). Images were obtained using an *S. carnosus* cell probe on top of a corneocyte at a scan area of 45 μm × 45 μm (256 pixels × 256 pixels), with an applied force of 0.5 nN, and a constant approach and retraction speed of 40 μm s^{-1} (z-range of 1 mm). For each condition, experiments were repeated for at least 3 different cell pairs.

Isothermal titration calorimetry

ITC experiments were performed[16] using a MicroCal VP-ITC microcalorimeter. Analysis and fitting were done with ORIGIN software. Sample cells contained 20 μM of lectin protein (1.5 mL) and the syringe contained 1 mM of glycan (450 μL). The heat response from twenty glycan injections was measured; the first injection was a volume of 2 μL and the subsequent nineteen injections were at a volume of 14 μL each.

Corneocyte collection

Desquamated corneocytes from the lower or upper arm near the elbow were collected from healthy human volunteers.[17] Clear, adhesive tape stripping discs (d-Squame D100; Clinical & Derm) were used to collect corneocytes following cleaning and air-drying of the collection area with an alcohol wipe.

Preparation of bacterial strains for corneocyte and N/TERT adhesion assays

All bacterial strains expressed superfolder green fluorescent protein (sGFP), either on plasmid pCM29 for *S. aureus* and *S. epidermidis* strains or chromosomally for *S. carnosus* strains.[17] Strains were grown overnight at 37°C with shaking aeration at 220 rpm in tryptic soy broth (TSB) in the presence of 10 μg/mL of chloramphenicol for plasmid maintenance. Strains were then sub-cultured at a 1:50 dilution in TSB with chloramphenicol and grown to an OD600 of ∼0.75. Strains were diluted to a final OD600 of 0.15 (∼10^7 colony-forming units [CFU]/mL) after washing once in PBS at a 1:1 ratio. An OD600 of 0.15 was chosen to allow for adequate cell enumeration without clumping of bacterial cells.[15,17]

Corneocyte adhesion assays

Co-incubation with purified glycans

SasG-II-expressing *S. carnosus-sasG*$_{MW2}$ was tested for adhesion to corneocytes following co-incubation with the purified glycans *N*-acetyl-D-lactosamine (Sigma-Aldrich) or 3′-sialyl-*N*-acetyllactosamine (Sigma-Aldrich). *N*-acetyl-D-lactosamine was prepared in PBS to a concentration of 1000 μM and diluted 2-fold from 1000 μM to 62.5 μM. 3′-Sialyl-*N*-acetyllactosamine was prepared in PBS to a concentration of 100 μM and diluted 2-fold from 100 μM to 6.25 μM. 300 μL of prepared glycans and 300 μL of prepared bacterial strains were co-incubated at room temperature for 20 min. The entire 600 μL was then incubated on corneocytes for 45 min at 37°C. *S. carnosus*-pALC2073 was used as a negative control.

Pre-incubation with glycosidases

S. carnosus strains expressing SasG-I (*S. carnosus-sasG*$_{COL}$) and SasG-II (*S. carnosus-sasG*$_{MW2}$) were tested for adhesion to corneocytes following deglycosylation. Corneocytes were incubated with one of the following glycosidases for 24 h at 37°C in a moist chamber: PNGase F, O-Glycosidase, α1-2,3,6 Mannosidase, α1-3,4 Fucosidase, β-*N*-Acetylglucosaminidase S, β1-4 Galactosidase S, and α2-3,6,8 Neuraminidase (NEB). A 300 μL total solution for each enzyme contained: 3 μL enzyme, 30 μL GlycoBuffer (specific to each enzyme), and 30 μL BSA supplement for α1-3,4 Fucosidase or 30 μL zinc supplement for α1-2,3,6 Mannosidase, and addition of PBS up to 300 μL. After 24 h, corneocytes were washed with PBS and subsequently incubated with the specified strains for 45 min at 37°C. Each of the prepared solutions without the enzymes were used as control conditions for each experimental group.

Pre-incubation/blocking with purified lectins

Strains with SasG-II, *S. aureus* MW2 and *S. carnosus*-SasG$_{MW2}$, were tested for adhesion to corneocytes following pre-incubation/blocking with purified recombinant lectins from Aap, Aap ΔY580A, SasG-I, SasG-I ΔW392A, and SasG-II. Lectins were prepared to a concentration of 5 μM in 300 μL PBS. The prepared lectins were incubated on corneocytes at room temperature for 20 min, followed by incubation with 300 μL prepared bacterial strains for 45 min at 37°C. *S. aureus* Δ*mgrA* Δ*sasG* or *S. carnosus*-pALC2073 (EV) were used as negative controls.

Pre-incubation/blocking with purified type II full-length SasG and SasG-II A-domain

S. epidermidis and SasG-I-expressing *S. carnosus-sasG*$_{COL}$ were tested for adhesion to corneocytes following pre-incubation with purified full-length SasG-II or purified A-domain from *S. aureus* MW2. 300 μL of purified protein were prepared in PBS at a concentration of 100 μg/mL and incubated on corneocytes for 45 min at room temperature, followed by incubation with 300 μL prepared bacterial strains at 37°C for 45 min. *S. epidermidis* Δ*ica* Δ*aap* or *S. carnosus*-pALC2073 (EV) were used as negative controls.

N/TERT adhesion assays

To study the adhesion of SasG to live host cells, immortalized N/TERT-2G keratinocytes were utilized.[46] Here, low passage (<10) undifferentiated N/TERT-2G cells were seeded to 1x10^5 cells/mL in either experiment media (EM)[46] or keratinocyte serum-free medium (KSFM, Gibco) in a 24-well tissue culture treated plate. For the assays on differentiated N/TERT-2G cells, the keratinocytes were both seeded in and allowed to differentiate in EM for 1 week with media changes every two days to promote the formation of a

stratified and thick layer of epithelial cells. For assays using undifferentiated N/TERT-2G cells, cells were seeded in KSFM and were allowed to form a 100% confluent monolayer (approximately 2–3 days growth) with daily media changes. All cells were grown at 37°C with 5% CO_2.

On the day of experimentation, cells were inoculated with *S. carnosus*-pALC2073 (EV), *S. carnosus-sasG*$_{MW2}$ (SasG-II), *S. carnosus-sasG*$_{COL}$ (SasG-I), or *S. carnosus-sasG*$_{MW2\Delta A}$ prepared in PBS. The growth media was removed, and each strain was inoculated onto N/TERT-2G cells in technical triplicate at an MOI of 5 using a total inoculum volume of 100 μL. Upon addition of bacteria, the bacteria were allowed to incubate on the cells for 30 min following a 5-min spin at 1000 rpm. After the 30-min incubation, the N/TERT-2G cells were gently washed three times with 500 μL of sterile PBS per well to remove any un-adhered bacteria. 100 μL of 0.05% trypsin-EDTA (Sigma-Aldrich) was then added to each well and allowed to incubate for 10 min at 37°C with 5% CO_2. The trypsinized cells were then resuspended in 400 μL sterile PBS, serially diluted, and plated to quantify the bacterial CFU/mL. Adhered bacterial cells were assessed as overall percent adhesion as well as percent cell association normalized to the *S. carnosus-sasG*$_{MW2}$ input inoculum.

Pre-incubation with glycosidases

S. carnosus strains expressing SasG-I (*S. carnosus-sasG*$_{COL}$) and SasG-II (*S. carnosus-sasG*$_{MW2}$) were tested for adhesion to differentiated N/TERT-2G keratinocytes following deglycosylation. Cells were seeded and allowed to differentiate for 1 week as described above. Cells were incubated with glycosidases β-*N*-Acetylglucosaminidase S and β1-4 Galactosidase S at a 1:100 ratio in KSFM for 24 h. After incubation, the cells were inoculated with the *S. carnosus* strains and followed the same adhesion and quantification protocol as described above.

QUANTIFICATION AND STATISTICAL ANALYSIS

For each experiment, the number of replicates (n) and manner of data presentation (definition of center and precision of measures) is provided in the figure legends. For all assays, data were pooled from at least two independent experiments. Description of statistical analyses and significance are provided in the figure legends for all applicable experiments. AFM data were analyzed using the data processing software from JPK Instruments (Berlin, Germany). Adhesion peaks were fitted using the worm-like chain (WLC) model. Rupture forces were then obtained from these fits, further analyzed, and plotted using Origin software. Differences in adhesion between strains for the corneocyte adhesion assays were analyzed using an unpaired t test, ordinary one-way ANOVA, or a non-parametric Mann-Whitney test. A p-value of ≤ 0.05 was considered significant. GraphPad Prism software was used for statistical calculations for the corneocyte adhesion assays.